RESEARCH ARTICLE | SEPTEMBER 26 2024

An analysis of a 2 × 2 Keyfitz–Kranzer type balance system with varying generalized Chaplygin gas *⊙*

J. Frew 🗓 ; N. Keyser 🗓 ; E. Kim 🗓 ; G. Paddock 🗓 ; C. Toumbleston 🗓 ; S. Wilson 🗓 ; C. Tsikkou 🗷 👵



Physics of Fluids 36, 096132 (2024) https://doi.org/10.1063/5.0231413





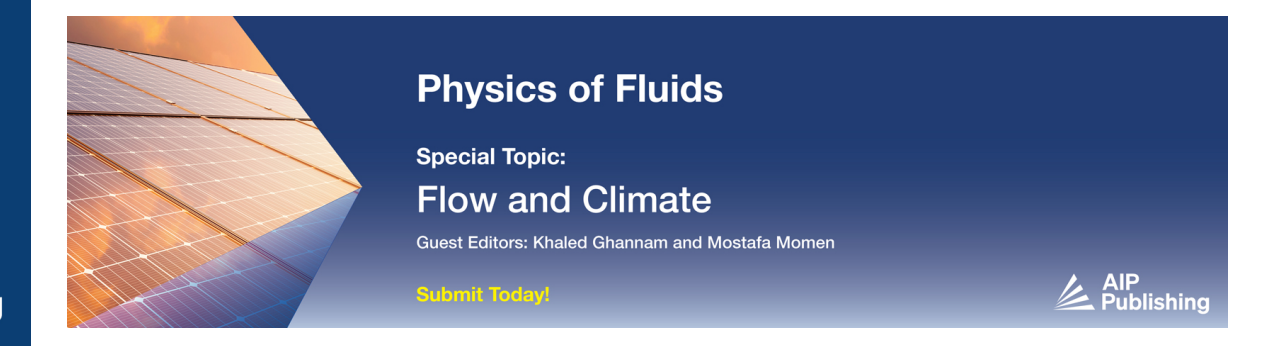
Articles You May Be Interested In

KoopmanLab: Machine learning for solving complex physics equations

APL Mach. Learn. (September 2023)

Experimental realization of a quantum classification: Bell state measurement via machine learning

APL Mach. Learn. (September 2023)





An analysis of a 2×2 Keyfitz-Kranzer type balance system with varying generalized Chaplygin gas

Cite as: Phys. Fluids **36**, 096132 (2024); doi: 10.1063/5.0231413 Submitted: 30 July 2024 · Accepted: 29 August 2024 · Published Online: 26 September 2024







View Online

J. Frew,^{1,a)} (b) N. Keyser,^{1,b)} (c) E. Kim,^{2,c)} (d) G. Paddock,^{3,d)} (d) C. Toumbleston,^{4,e)} (d) S. Wilson,^{5,f)} (d) and C. Tsikkou^{6,g)} (e)

AFFILIATIONS

- ¹Department of Mathematics, The Ohio State University, Columbus, Ohio 43210, USA
- 2 Department of Applied Physics and Applied Mathematics, Columbia University, New York City, New York 10027, USA
- ³Department of Mathematics, Virginia Tech, Blacksburg, Virginia 24060, USA
- Department of Mathematics, North Carolina State University, Raleigh, North Carolina 27606, USA
- Department of Mathematics, University of Pittsburgh, Pittsburgh, Pennsylvania 15260, USA
- ⁶School of Mathematical and Data Sciences, West Virginia University, Morgantown, West Virginia 26506, USA
- a) Electronic mail: frew.25@osu.edu
- b) Electronic mail: keyser.88@osu.edu
- c) Electronic mail: etk2124@columbia.edu
- d)Electronic mail: griffinmilo@vt.edu
- e) Electronic mail: cstoumbl@ncsu.edu
- f)Electronic mail: srw81@pitt.edu
- g)Author to whom correspondence should be addressed: tsikkou@math.wvu.edu

ABSTRACT

We consider a system of two balance laws of Keyfitz–Kranzer type with varying generalized Chaplygin gas, which exhibits negative pressure and is a product of a function of time and the inverse of a power of the density. The Chaplygin gas is a fluid designed to accommodate measurements for the early universe and late-time universal expansion while obeying the pressure–density–time relation. We produce an explanation and description of the non-self-similar Riemann solutions, including the non-classical singular solutions. We also find that due to a direct dependence on time, a change in the regions allowing for combinations of classical and non-classical singular solutions occurs; therefore, a Riemann solution can have different solutions over several time intervals. Our findings are confirmed numerically using the Local Lax–Friedrichs scheme.

Published under an exclusive license by AIP Publishing. https://doi.org/10.1063/5.0231413

I. INTRODUCTION

It is well accepted that dark energy plays a critical role in the current expansion of the universe, in particular, the shift from deceleration to acceleration in the current epoch. Connections between dark energy and dark matter are still debated in the physics community; the Chaplygin gas models are possible candidates for such connections, exhibiting early behavior akin to dark matter and later behavior akin to a cosmological constant. All Chaplygin gas models are unified in describing dark energy through scalar fields with a negative pressure and inverse relation density of the form $p = A/\rho$, where A < 0. Of particular interest are the varying and generalized Chaplygin gas models. ^{1,2} The former is characterized by the equation of state $p = B(t)/\rho$. Recently, Khurshudyan proposed the idea of setting $B(t) = Ae^{\eta t}$, where η and A < 0 are constants. He showed that this form describes the

quasi-exponential phase of the universe. Li³ built upon this work by analyzing the system of balance laws formed from a mathematical viewpoint. The generalized Chaplygin gas is characterized by the equation of state $P=A\rho^\gamma$, with $\gamma<0.^4$ To the best of our knowledge, there has been little research on a combination of both the varying and generalized model, denoted by the varying generalized Chaplygin gas (VGCG) model

This paper aims to study the solutions to the Riemann problem, an initial value problem that consists of data containing two constant states separated by a discontinuity at the origin, to a non-symmetric Keyfitz–Kranzer type system:

$$\begin{cases} \rho_t + (\rho(u - p(\rho)))_x = k\rho, \\ (\rho u)_t + (\rho u(u - p(\rho)))_x = \eta \rho u + \beta \rho, \end{cases}$$
(1.1)

where $A<0,k,\eta$, and β are non-zero physical constants. The independent variables are time $t\in\mathbb{R}^+$ and position $x\in\mathbb{R}$, and the dependent variables are density ρ and fluid velocity u. We restrict attention to $p(\rho)=A\rho^\gamma e^{\eta t}$, with $\gamma<0$, $(\gamma\neq-1)$ and $\rho(x,t)>0$. We refer the reader to Li³ for the special case $\gamma=-1$. In particular, we focus on the existence of singular solutions (delta or singular shocks), which denote the mass' concentration process and may be interpreted as galaxies in the universe. The non-autonomous system of balance laws (1.1) is of great interest mathematically and physically, as the solutions are non-self-similar, and the shock and rarefaction-type curves change over time. To the best of our knowledge, direct time dependence resulting in changes in the areas where classical and non-classical singular solutions exist has not been analyzed and confirmed numerically before.

The singular solutions involve the so-called delta or singular shocks, a more compressive generalization of the ordinary shock wave, where at least one state variable develops an extreme concentration in the form of a weighted Dirac delta function. They were initially discovered by Keyfitz and Kranzer⁵⁻⁷ and later studied in greater depth by Sever.8 Keyfitz and Kranzer5 worked with a strictly hyperbolic, genuinely nonlinear system derived from a one-dimensional model for isothermal gas dynamics and observed that there is a large region where the Riemann problem cannot be solved using shocks and rarefactions. They produced approximate unbounded solutions that do not satisfy the equation in the classical weak-solution sense. They also showed that only the first component of the Rankine-Hugoniot relation is satis field, giving a unique speed σ for which any given two states can be joined. Later on, Schecter⁹ used ideas and methods associated with dynamical systems with geometric flavor (blowing-up approach to geometric singular perturbation problems that lack normal hyperbolicity; see Fenichel¹⁰ and Jones¹¹) to prove the existence of a self-similar viscous solution. See also Hsu, 12 Kalisch et al., 13 Keyfitz et al., 14-Levine et al., 18 Mavromoustaki et al., 19 and references therein for other solutions involving singular solutions.

The investigation of singular solutions was mainly focused on when only one state variable develops the Dirac delta function, and the others are functions with a bounded variation. We have other physically important systems with delta functions in more than one state variable. For example, Mazzotti *et al.*^{20–22} numerically studied a model with important applications in modern industry, which exhibits singular solutions arising in two-component chromatography, and both components of the Rankine–Hugoniot relation are not satisfied. Tsikkou²³ considered this chromatography system, which exhibits a change of type (hyperbolic and elliptic), performed linear changes in the conserved quantities to obtain a simpler system, and gave a coherent explanation and description of the unbounded solutions.

It is natural to then ask whether it is possible to predict singular solutions to a system, find a physical interpretation of their significance, explain the sense in which they satisfy the equation, find a better definition that will describe some broader collection of examples, and check for connections between singular solutions, genuinely nonlinear systems, and change of type (conservation laws which are not everywhere hyperbolic). The model under consideration serves this purpose in addition to the aforementioned physical reasons. From a mathematical point of view, we aim to gain a broader perspective for solving Riemann and Cauchy problems with large data globally using singular solutions as additional building blocks (in possibly generalized schemes).

The system (1.1) is a special case of

$$\begin{cases} \rho_t + (\rho \Phi(\rho, u))_x = F(\rho, u), \\ (\rho u)_t + (\rho u \Phi(\rho, u))_x = G(\rho, u), \end{cases}$$
(1.2)

where $\Phi(\rho,u)=f(u)-p(\rho)$ is a nonlinear function and has various applications depending on Φ,F , and, G. For example, the pressureless Euler system and the macroscopic model for traffic flow by Aw and Rascle²⁴ correspond to F=G=0, $\Phi(\rho,u)=u$, and F=G=0, f(u)=u. The literature^{25,26} shows that the Riemann problem with pressure laws depending only on the density and F=0 has been well studied. Motivated by Li^3 and references therein, we consider system (1.1) with initial data

$$(\rho, u)(x, 0) = \begin{cases} (\rho_L, u_L), & \text{if } x < 0, \\ (\rho_R, u_R), & \text{if } x > 0. \end{cases}$$
 (1.3)

The paper is organized as follows: In Sec. II, we use the following substitution:

$$\rho = ve^{kt}, \quad u = w + \beta t, \tag{1.4}$$

$$\rho = ve^{kt}, \quad u = \left(w + \frac{\beta}{\eta - k}\right)e^{(\eta - k)t} - \frac{\beta}{\eta - k},\tag{1.5}$$

for $\eta=k$ and $\eta\neq k$, respectively, to transform (1.1) to a system of conservation laws and present the numerical method used to verify our analytical results. Section III gives a formal description of the classical Riemann solutions to the system of conservation laws. We use the Rankine–Hugoniot relations to derive the shock curves through a left state and the method of characteristics to get information about the rarefaction-type curves. All the curves depend on time; therefore, various regions where classical Riemann solutions (using one-shock, two-contact discontinuity, and two-rarefaction) exist evolve in time. On the other hand, the Riemann solution with the right state in region V consists of delta-shocks. In Sec. IV, we prove that the singular solution satisfies (1.1) in the sense of distributions and we discuss the region time evolution. In Sec. V, we construct the singular solution to the Riemann problem for the original system (1.1), and finally, in Sec. VI, we present the conclusion.

II. PRELIMINARIES

A. Analysis preliminaries

The problem is best split into two cases: $\eta \neq k$ and $\eta = k$. For the $\eta \neq k$ case, the change of variables in (1.5) with the restriction $\nu > 0$ is used. With this, we rewrite (1.1) into the resulting conservative system

$$\begin{cases} v_t + \left[ve^{(\eta - k)t} \left(w + \frac{\beta}{\eta - k} \right) - v \frac{\beta}{\eta - k} - A(ve^{kt})^{\gamma + 1} e^{(\eta - k)t} \right]_x = 0, \\ \left[v \left(w + \frac{\beta}{\eta - k} \right) \right]_t + \left[v \left(w + \frac{\beta}{\eta - k} \right)^2 e^{(\eta - k)t} \\ - \left(w + \frac{\beta}{\eta - k} \right) e^{(\eta - k)t} A(ve^{kt})^{\gamma + 1} - \frac{\beta}{\eta - k} \left(w + \frac{\beta}{\eta - k} \right) v \right]_x = 0. \end{cases}$$

$$(2.1)$$

For the other case, $\eta=k$, the transformations in (1.4) with restriction $\nu>0$ are used. This results in

$$\begin{cases} v_t + \left[v(w+\beta t) - A(ve^{kt})^{\gamma+1}\right]_x = 0, \\ \left(vw\right)_t + \left[v(w+\beta t)w - A(ve^{\eta t})^{\gamma+1}w\right]_x = 0. \end{cases}$$
 (2.2)

Due to (1.3), the initial conditions for both systems are

$$(v, w)(x, 0) = (\rho, u)(x, 0) = \begin{cases} (v_L, w_L), & \text{if } x < 0, \\ (v_R, w_R), & \text{if } x > 0, \end{cases}$$

$$= \begin{cases} (\rho_L, u_L), & \text{if } x < 0, \\ (\rho_R, u_R), & \text{if } x > 0. \end{cases}$$
 (2.3)

B. Numerical preliminaries

The Local Lax-Friedrichs (LLF) scheme was utilized for its simplicity and non-oscillatory behavior. Following the scheme, the spatial and temporal domains were discretized. Neumann boundary conditions were imposed to preserve the left and right states of the solution at the end points. In particular, the (n + 1)th temporal solutions were calculated from the neighboring nth solutions and fluxes following from the equation:

$$U_j^{n+1} = \frac{1}{2} (U_{j-1}^n + U_{j+1}^n) + \frac{\text{CFL}}{2\lambda} (F_{j+1}^n - F_{j-1}^n), \tag{2.4}$$

where CFL represents a numerical stability condition for the LLF scheme given by the inequality

$$\frac{\Delta t}{\Delta x}\lambda \le \frac{1}{2} \tag{2.5}$$

in which λ represents the maximum wave speed given by the system eigenvalues. By construction $\Delta t = \frac{\text{CFL}}{\lambda}$, thus automatically satisfying the CFL condition with $\Delta x = 1$. Also note satisfying the CFL conditions guarantees that the LLF scheme converges to the physically correct weak solution satisfying entropy conditions.²⁷ Additionally, our selection of parameters optimized our simulation by increasing precision and eliminating potentially oscillatory and unstable behavior. In particular, we imposed the following conditions:

- |A| > 10 as the magnitude of A can be shown to be directly related to the size of the regions. Note that for large magnitudes of A, some regions become difficult to access. Alternatively, too small of a magnitude for case 1 results in regions that are too small to be insightful. It was imperative to examine the behavior of the regions graphically beforehand to ensure selected points tested the desired behaviors.
- |k| = 0.01 or |k| = 0.6 due to the term e^{kt} present in C_2 and R_2 . The parameter k controls the rate at which the curves change in

time and, therefore, the regions. The former leads to curves that undergo minimal change in time, allowing insight into the initial combinations to enter regions. The latter approximates longterm behavior in time, modeling regional collapse. Note that even for |k| = 0.6, regional collapse happens within the numerical temporal domain.

• While η alone does not have a strong effect on region behavior, we require $\eta - k > 0$ due to the factor of $e^{(n-k)t}$ in λ_1 and λ_2 . If $\eta - k < 0$, $\lim_{t \to \infty} e^{(n-k)t} = 0$, causing $\lambda_1 = \lambda_2$ as $t \to \infty$. We thus lose hyperbolicity of our regions, resulting in the breakdown of our implementation to unexpected behavior.

Note that we only discuss A, η , and k here, as β has minimal effect on qualitative numerical results.

To further prevent numerical instability, the change of variables $y = vw + v\frac{\beta}{\eta - k}$ was utilized in our implementation. Thus, the vector of conserved quantities is $H = \begin{bmatrix} v & y \end{bmatrix}^T$ and the flux is written directly in terms of y. We then converted y back to w with each iteration.

Note that for all numerical figures, $U_L = \begin{bmatrix} v_L & w_L \end{bmatrix}^T$ and $U_R = \begin{bmatrix} v_R & w_R \end{bmatrix}^T$. See also LeVeque *et al.*^{28,29} for additional details on

the LLF scheme.

III. CONTACT DISCONTINUITY, SHOCK, AND RAREFACTION

This section is broken into two cases: $\eta \neq k$ and $\eta = k$. Each case begins by finding the Hugoniot locus, using the Rankine-Hugoniot condition to find the set of points in state space that may be joined to a fixed left state by a shock satisfying the Lax shock admissibility criterion or contact discontinuity. In addition, using the method of characteristics, we show that one-rarefactions cannot exist and derive information about the two-rarefactions. Next, numerical evidence of the latter is presented and analyzed. Finally, the Hugoniot locus and rarefaction-type curve are plotted together, splitting the (v, w) state space into regions depending on γ and k. Note that numerical evidence is only presented for the $\eta \neq k$ case due to the regions being identical in both cases.

A. $\eta \neq k$ case

1. Hyperbolicity, linear degeneracy, and genuine nonlinearity

(2.1) is rewritten as

$$H_t + G_r = 0, (3.1)$$

where

$$\begin{cases}
H = \begin{bmatrix} v \\ vw + v \frac{\beta}{\eta - k} \end{bmatrix}, \\
G = \begin{bmatrix} ve^{(\eta - k)t} \left(w + \frac{\beta}{\eta - k} \right) - v \frac{\beta}{\eta - k} - A(ve^{kt})^{\gamma + 1} e^{(\eta - k)t} \\ v \left(w + \frac{\beta}{\eta - k} \right)^2 e^{(\eta - k)t} - \left(w + \frac{\beta}{\eta - k} \right) e^{(\eta - k)t} A(ve^{kt})^{\gamma + 1} - \frac{\beta}{\eta - k} \left(w + \frac{\beta}{\eta - k} \right) v \end{bmatrix}.
\end{cases}$$
(3.2)

To check whether our system is hyperbolic, we need

$$\begin{cases}
DH = \begin{bmatrix} 1 & 0 \\ w + \frac{\beta}{\eta - k} & v \end{bmatrix}, \\
Equation & \begin{cases}
e^{(\eta - k)t} \left(w + \frac{\beta}{\eta - k} \right) - \frac{\beta}{\eta - k} - A(ve^{kt})^{\gamma} e^{(\eta - k)t} (\gamma + 1) & ve^{(\eta - k)t} \\
0 & \begin{cases}
w + \frac{\beta}{\eta - k} \\ -\frac{\beta}{\eta - k} \\ w + \frac{\beta}{\eta - k} \\ w + \frac{\beta}$$

where D denotes the differential $[\partial/\partial v, \partial/\partial w]$. Solving det(DG $-\lambda DH$) = 0 to obtain the eigenvalues of the system yields

$$\begin{cases} \lambda_1 = \frac{-\beta}{\eta - k} + \left[w + \frac{\beta}{\eta - k} - \frac{A}{v} (ve^{kt})^{\gamma + 1} (\gamma + 1) \right] e^{(\eta - k)t}, \\ \lambda_2 = \frac{-\beta}{\eta - k} + \left[w + \frac{\beta}{\eta - k} - \frac{A}{v} (ve^{kt})^{\gamma + 1} \right] e^{(\eta - k)t}. \end{cases}$$
(3.4)

The corresponding eigenvectors are

$$\begin{cases}
r_1 = \begin{bmatrix} 1 \\ 0 \end{bmatrix}, \\
r_2 = \begin{bmatrix} \frac{A\gamma}{v^2} (ve^{kt})^{\gamma+1} \end{bmatrix}.
\end{cases}$$
(3.5)

Here we note that A < 0 and $\gamma < 0$ gives $\lambda_1 < \lambda_2$. Furthermore, observe that

$$\begin{cases} D\lambda_{1} \cdot r_{1} = \frac{A}{v^{2}} (\gamma + 1) (ve^{kt})^{\gamma} e^{\eta t} (-v\gamma) \neq 0, \\ D\lambda_{2} \cdot r_{2} = \frac{A}{v^{2}} (ve^{kt})^{\gamma} e^{\eta t} (-v\gamma) + e^{(\eta - k)t} \frac{A\gamma}{v^{2}} (ve^{kt})^{\gamma + 1} = 0. \end{cases}$$
(3.6)

Hence, the one- and two-characteristic families are genuinely nonlinear and linearly degenerate, respectively.

2. Hugoniot locus through a left state (v_-, ω_-): The Lax shock admissibility criterion

Let $\sigma(t) = x'(t)$ be the propagation speed. Using the Rankine-Hugoniot jump conditions,

$$\begin{cases} -\sigma(t)[v]_{\text{jump}} + \left[ve^{(\eta-k)t}\left(w + \frac{\beta}{\eta-k}\right) - v\frac{\beta}{\eta-k} - A(ve^{kt})^{\gamma+1}e^{(\eta-k)t}\right]_{\text{jump}} = 0, \\ -\sigma(t)\left[vw + \frac{v\beta}{\eta-k}\right]_{\text{jump}} + \left[v\left(w + \frac{\beta}{\eta-k}\right)^{2}e^{(\eta-k)t} - \left(w + \frac{\beta}{\eta-k}\right)e^{(\eta-k)t}A(ve^{kt})^{\gamma+1} - \frac{\beta}{\eta-k}\left(w + \frac{\beta}{\eta-k}\right)v\right]_{\text{jump}} = 0, \end{cases}$$

$$(3.7)$$

where $\left[\cdot\right]_{jump}$ denotes the jump across the shock, we conclude that the states that can be connected to (v_-, w_-) by a one-shock or a twocontact discontinuity lie on the curves

$$S_1(v_-, w_-) : w = w_-$$
 (3.8)

$$C_2(v_-, w_-) : w = w_- - \frac{A}{v_-} (v_- e^{kt})^{\gamma+1} + \frac{A}{v_-} (v_- e^{kt})^{\gamma+1},$$
 (3.9)

respectively. These two curves intersect at (v_-, w_-) . By (3.7), we get

$$\sigma_{1}(t) = \left(w_{-} + \frac{\beta}{\eta - k}\right) e^{(\eta - k)t} - \frac{\beta}{\eta - k} -Ae^{(\eta - k)t} e^{k(\gamma + 1)t} \frac{v^{\gamma + 1} - v_{-}^{\gamma + 1}}{v - v_{-}},$$

$$\sigma_{2}(t) = \lambda_{2}(v, w) = \lambda_{2}(v_{-}, w_{-}).$$
(3.10)

For the one-shock to satisfy the Lax shock admissibility criterion, we require

$$\lambda_1(v_-, w_-) > \sigma_1 > \lambda_1(v, w).$$
 (3.11)

$$\begin{cases}
h_1(v) < 0, & h_2(v) > 0 & \text{when } v > v_-, \\
h_1(v) > 0, & h_2(v) < 0 & \text{when } v < v_-,
\end{cases}$$
(3.12)

which hold when

$$-1 < \gamma < 0, \quad \gamma < -1,$$

respectively. This can be easily checked by studying the first and second derivatives of h_1 and h_2 . Therefore, the admissible parts of the one-shock curve consist of points with $v>v_-$ when $-1<\gamma<0$ and points with $v < v_{-}$ when $\gamma < -1$.

3. One-rarefaction-type curve through a left state (v_-,ω_-)

Recall Eqs. (3.4) and (2.1). Differentiating (2.1) and then simplifying with (3.4) yield

$$w_t + \lambda_2 w_x = 0, v_t + \lambda_1 v_x + v w_x e^{(\eta - k)t} = 0.$$
 (3.13)

We rewrite these equations in matrix form to get

$$\begin{bmatrix} v_t \\ w_t \end{bmatrix} + \begin{bmatrix} \lambda_1 & ve^{(\eta - k)t} \\ 0 & \lambda_2 \end{bmatrix} \begin{bmatrix} v_x \\ w_x \end{bmatrix} = 0.$$
 (3.14)

Note that the eigenvalues and eigenvectors of the matrix $A = \begin{bmatrix} \lambda_1 & ve^{(\eta-k)t} \\ 0 & \lambda_2 \end{bmatrix}$ are the same as (3.4) and (3.5).

The matrix A is diagonalized in the form PDP^{-1} where

$$D = \begin{bmatrix} \lambda_1 & 0 \\ 0 & \lambda_2 \end{bmatrix}, \tag{3.15}$$

$$P = \begin{bmatrix} 1 & v^2 \\ 0 & \gamma A (ve^{kt})^{\gamma+1} \end{bmatrix}, \tag{3.16}$$

and

$$P^{-1} = \begin{bmatrix} 1 & \frac{-v^2}{\gamma A (ve^{kt})^{\gamma+1}} \\ 0 & \frac{1}{\gamma A (ve^{kt})^{\gamma+1}} \end{bmatrix}.$$
 (3.17)

These matrices are now used to transform Eq. (3.14) into

$$P^{-1} \begin{bmatrix} v_t \\ w_t \end{bmatrix} + DP^{-1} \begin{bmatrix} v_x \\ w_x \end{bmatrix} = 0, \tag{3.18}$$

which yields

$$w_t + \lambda_2 w_x = 0,$$

$$v_t + \lambda_1 v_x - \frac{v^2}{\gamma A (v_e^{kt})^{\gamma + 1}} (w_t + \lambda_1 w_x) = 0.$$
(3.19)

This implies that $\frac{dw}{dt} = 0$ along two-characteristics, that is $\frac{dx}{dt} = \lambda_2$, and thus w is constant. On the other hand, along one-characteristics where $\frac{dx}{dt} = \lambda_1$, we get

$$\frac{dw}{dt} = A\gamma v^{\gamma - 1} e^{kt(\gamma + 1)} \frac{dv}{dt}.$$
 (3.20)

As discussed above, when we consider a one-rarefaction-type wave connecting the constant left state (v_-, w_-) with another state (see Fig. 1 as an illustrative example), w would be constant and equal to w_- in directions given by $\frac{dx}{dt} = \lambda_2$.

Therefore, w would stay constant throughout this wave and by (3.20) v would also stay constant since $\frac{dw}{dt} = 0$ implies $\frac{dv}{dt} = 0$. By the method of characteristics, we thus conclude that a one-rarefaction does not exist.

4. Two-rarefaction-type curve through a left state (v_-,ω_-)

We note that for numerical figures the left column displays all 20 iterations, each taking 1000 steps, while the right column displays the latest iteration. Data were renormalized every 100 steps within an error bound of 10^{-7} to remove illusory points. Later iterations have a thicker line width. The figures are provided to justify the existence of two-rarefaction-type waves numerically. Sections III A 5, III A 6, and III B will discuss the regions and cases mentioned in the figure captions.

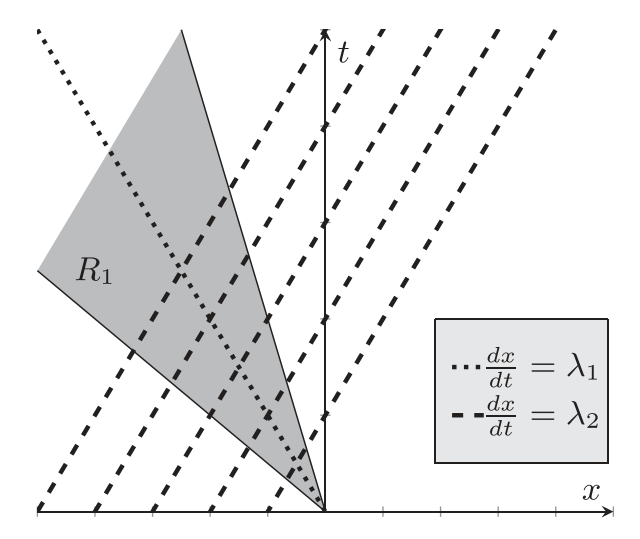


FIG. 1. An illustration of the characteristics for a hypothetical one-rarefaction-type wave

From testing various points, it was found that R_2 lies tightly along C_2 . Numerically, we observed strictly R_2C_2 (the Riemann solution consists of a two-rarefaction followed by a two-contact discontinuity) when R_2 is present for all points tested, but cannot confirm this analytically. Note that the change in w during R_2 is extremely small, appearing zero graphically.

With numerical assurance for a R_2 rarefaction, we proceed to analyze its behavior. From (3.20), we can measure the rate of change of w with respect to t on the curve. Since the system is non-autonomous, it is difficult to find the two-rarefaction-type curve explicitly. First, we note that a two-rarefaction $R_2(v_-, w_-)$ lies above $C_2(v_-, w_-)$; to connect a left state (v_-, w_-) with another state (v_-, w_-) without crossing characteristics, we require $\lambda_2(v_-, w_-) < \lambda_2(v_-, w_-)$, ensuring diverging characteristics, as is expected for a rarefaction. To pinpoint the location of R_2 , we differentiate (3.9) along $\frac{dx}{dt} = \lambda_1$ to get

$$\frac{dw}{dt}\Big|_{\text{across }C_2} = A\gamma v^{\gamma-1} e^{kt(\gamma+1)} \frac{dv}{dt} + Ak(\gamma+1) e^{kt(\gamma+1)} (v^{\gamma} - v_{\perp}^{\gamma}).$$
(3.21)

Note that since a rarefaction-type wave R_2 is a smooth solution, we can use (3.20)

$$\frac{dw}{dt}\Big|_{\text{across }R_2} = A\gamma v^{\gamma-1} e^{kt(\gamma+1)} \frac{dv}{dt}$$
 (3.22)

to study the behavior along one-characteristics. Consequently,

$$\begin{cases} \frac{dw}{dt} \Big|_{\arccos C_2} < A\gamma v^{\gamma - 1} e^{kt(\gamma + 1)} \frac{dv}{dt} & \text{when } k(\gamma + 1) > 0, \\ v < v_- & \text{or } k(\gamma + 1) < 0, v > v_-, \end{cases}$$

$$\begin{cases} \frac{dw}{dt} \Big|_{\arccos C_2} > A\gamma v^{\gamma - 1} e^{kt(\gamma + 1)} \frac{dv}{dt} & \text{when } k(\gamma + 1) > 0, \\ v > v & \text{or } k(\gamma + 1) < 0, v < v \end{cases}$$

$$(3.23)$$

Upon comparing the rates of change of w with respect to t (note that the rates are positive or negative when $v < v_-$ or $v > v_-$, respectively) on the two-waves we conclude that when $k(\gamma+1) < 0$ the two-rarefaction-type curve R_2 lies above the two-contact discontinuity C_2 when $v < v_-$. On the other hand, when $k(\gamma+1) > 0$, the two-rarefaction-type curve R_2 lies above C_2 when $v > v_-$.

Finally, with the assumption that the R_2 curve would follow closely above the C_2 curve, integration of (3.20) will give a non-explicit equation for R_2 as

$$w = w_{-} + Av^{\gamma}e^{kt(\gamma+1)} - Av_{-}^{\gamma}e^{kt_{0}(\gamma+1)} - \int_{t_{0}}^{t}v^{\gamma}Ak(\gamma+1)e^{kt(\gamma+1)}dt,$$
(3.24)

which is in line with the numerical analysis (see Figs. 2 and 3).

These together yield a rough outline of where the R_2 curve is located, given by the dotted line in Figs. 4–7. This is based off the similarity of (3.24) to the equation for C_2 , as well as the necessary high proximity to C_2 to observe R_2C_2 instead of S_1R_2 numerically. A full derivation of this equation is a topic of future work.

All results and analysis of the R_2 are expected to hold true for the $\eta=k$ case, due to the inequalities found for the $\eta\neq k$ case reappearing in the former.

5. Regions for the solution of the Riemann problem

The curves of our one-shock S_1 and two-contact discontinuity C_2 are given by (3.8) and (3.9).

The regions are defined further by

$$S_{\delta}$$
: $w = w_L + \frac{A}{r} (ve^{kt})^{\gamma+1}$, (3.25)

representing the limit of the second curve (3.9) as $v_L \to \infty$. Additionally, we have

$$S_o: w = w_L + \frac{A}{v} (ve^{kt})^{\gamma+1} - \frac{A}{v_I} (\gamma + 1) (v_L e^{kt})^{\gamma+1}, \qquad (3.26)$$

representing the max bound of the overcompressive region, which is explained in more detail in Sec. IV A 1. R_2 and all other unknown curves are represented by dotted lines in the (v, w) plane.

We distinguish four cases:

- Case 1, when $\gamma < -1$, k > 0, given by Fig. 4,
- Case 2, when $-1 < \gamma < 0, k < 0$, given by Fig. 5,
- Case 3, when $\gamma < -1$ and k < 0 given by Fig. 6,
- Case 4, when $-1 < \gamma < 0$ and k > 0, given by Fig. 7.

For each case, various regions exist that lead to classical and nonclassical solutions to the Riemann problem. Specifically, we have:

• A one-shock followed by a two-contact discontinuity. The former, given by $x = x_1(t)$, connects (v_L, w_L) and a middle state (v_M, w_M) , and the latter, given by $x = x_2(t)$, connects the middle state with the right state (v_R, w_R) . The middle state can be found explicitly by using (3.8) and (3.9):

$$w_M = w_L, \quad v_M(t) = \left(v_R e^{kt(\gamma+1)} + \frac{w_L - w_R}{A}\right)^{1/\gamma} e^{-kt(\gamma+1)/\gamma}.$$

In addition, by (3.10), we can find the wave speeds

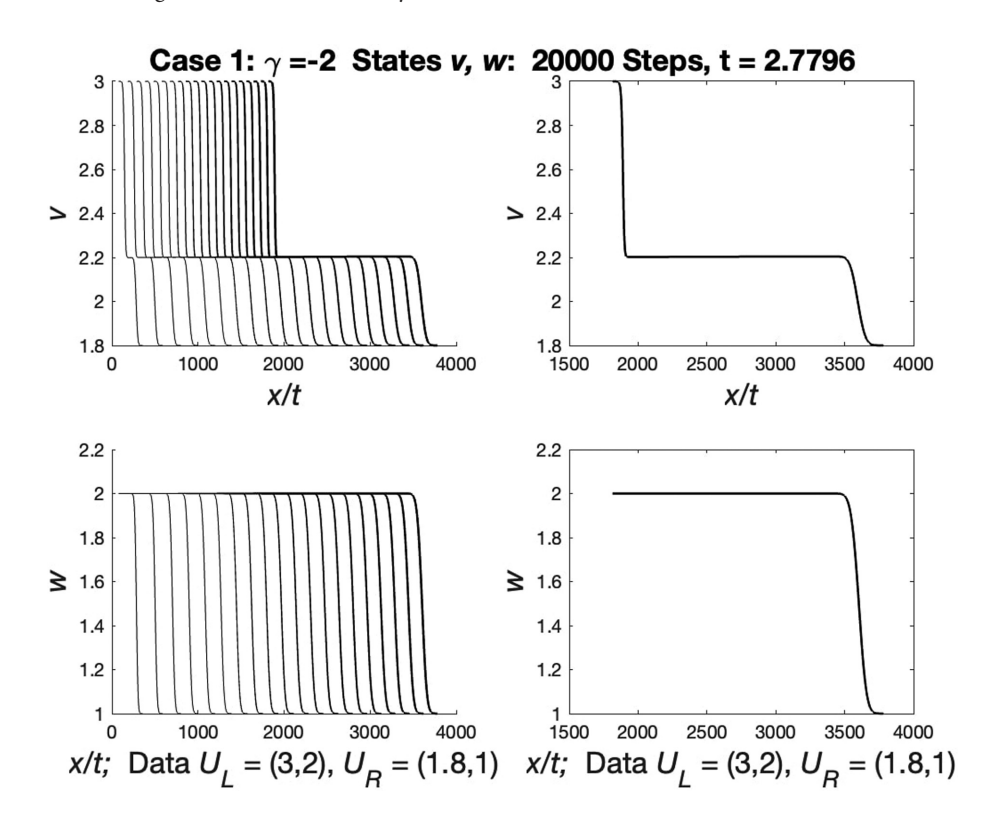


FIG. 2. Region VII in Fig. 4. S_1R_2 . Parameters: $\gamma=-2, A=-10, \eta=3, k=0.01, \beta=10.$

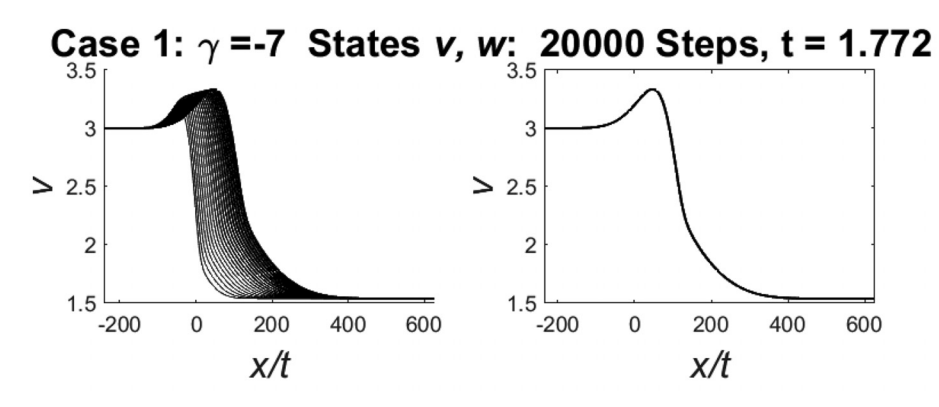
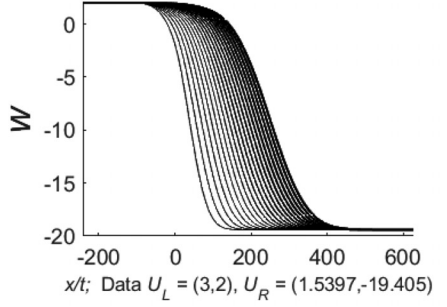
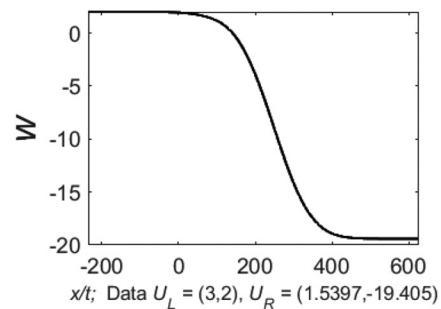


FIG. 3. Region VIII in Fig. 4. R_2C_2 . Parameters: $\gamma=-7, A=-500, \eta=3, k=0.01, \beta=10.$





$$\frac{dx_{1}}{dt} = \left(w_{L} + \frac{\beta}{\eta - k}\right) e^{(\eta - k)t} - \frac{\beta}{\eta - k} \\
-Ae^{(\eta - k)t} e^{kt(\gamma + 1)} \frac{v_{M}(t)^{\gamma + 1} - v_{L}^{\gamma + 1}}{v_{M}(t) - v_{L}}, \qquad (3.27)$$

$$\frac{dx_{2}}{dt} = \frac{-\beta}{\eta - k} + \left[w_{R} + \frac{\beta}{\eta - k} - \frac{A}{v_{R}} (v_{R} e^{kt})^{\gamma + 1}\right] e^{(\eta - k)t}.$$

This solution is possible when the right state is in region VI (case 1), given by Fig. 8, or region VII (case 3), given by Fig. 9, and region III or IV (cases 2 and 4) (see Figs. 10–13). The regions

- are bounded by $S_1(v_L, w_L)$ and $C_2(v_L, w_L)$ or S_δ and $C_2(v_L, w_L)$, respectively.
- A one-shock followed by a two-rarefaction. The solution is possible when the right state is in region VII (case 1), given by Fig. 14, or region VI (case 3), given by Fig. 15. The regions are bounded by $S_1(v_L, w_L)$ and $R_2(v_L, w_L)$.
- A two-rarefaction followed by a two-contact discontinuity, which is possible when the right state is in region I (cases 2 and 4), given, for example, by Figs. 16 and 17. The region is bounded by $C_2(v_L, w_L)$ and $R_2(v_L, w_L)$.

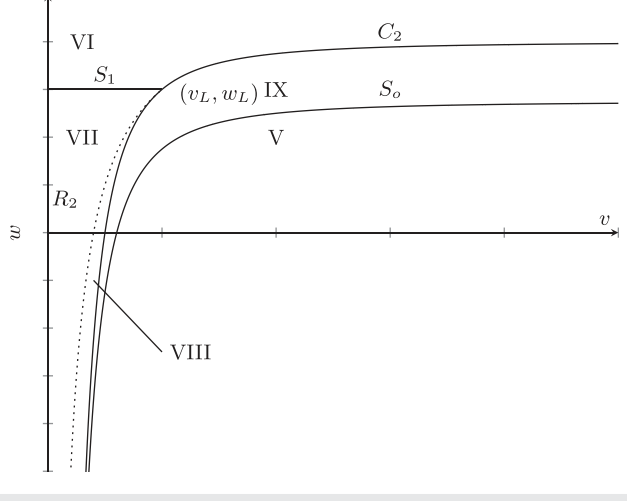


FIG. 4. Regions for $\gamma < -1$ and k > 0.

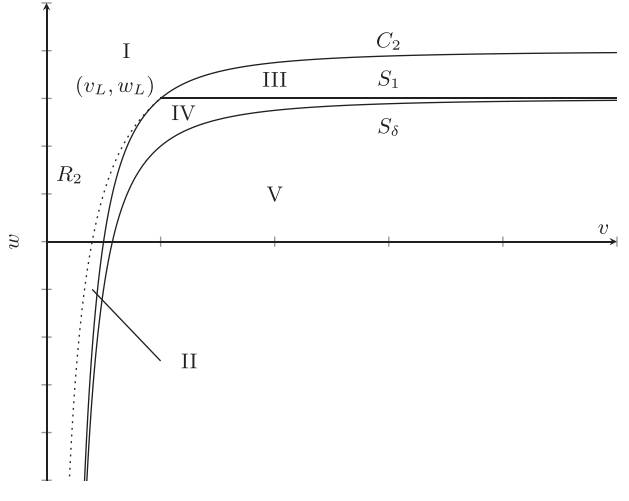


FIG. 5. Regions for $-1 < \gamma < 0$ and k < 0.

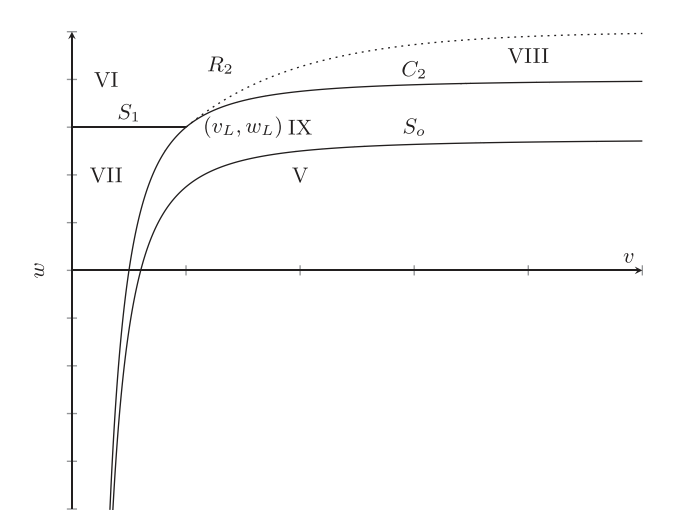


FIG. 6. Regions for $\gamma < -1$ and k < 0.

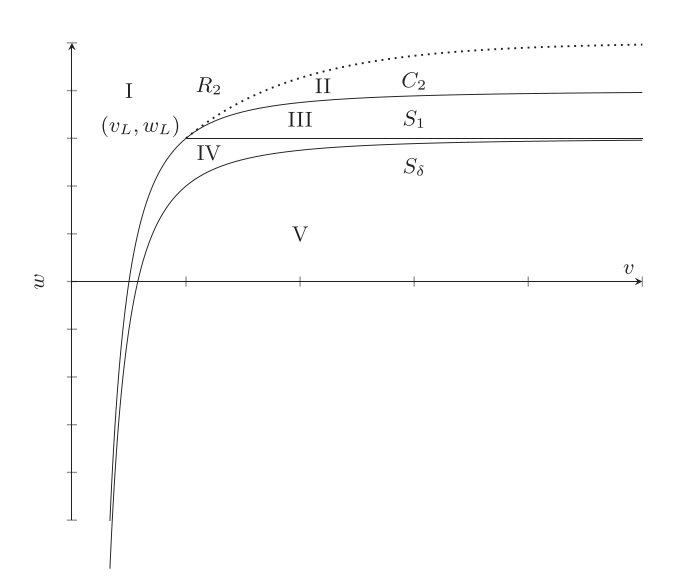


FIG. 7. Regions for $-1 < \gamma < 0$ and k > 0.

- A two-rarefaction followed by a two-contact discontinuity or vice versa. The region is bounded by $C_2(v_L, w_L)$ and $R_2(v_L, w_L)$. This is possible when the right state is in region VIII (case 1 and case 3) or region II (case 2 and case 4). Numerically, we find that the two-rarefaction comes first in region VIII in Fig. 4 and expect the same for region VIII in Fig. 6. However, due to the growth of C_2 into a vertical line during the region shift discussed later, picking a point adequately close to C_2 to observe behavior causes the point to almost immediately leave the region, making it impossible to verify. Further work needs to be done to tell if the two-rarefaction or the two-contact discontinuity occurs first.
- A delta-shock that is overcompressible and possible when the right state is in the overcompressive subset of region V (cases 1–4). The region is bounded by either S_{δ} (cases 2 and 4) or S_{o} (cases 1 and 3). Overcompressibility will be discussed in Sec. IV A 1.

• Either a delta-shock followed by a two-wave or a two-contact discontinuity followed by a delta-shock. This is possible in region IX (cases 1 and 3), which is bounded by $C_2(v_L, w_L)$ and S_o , and in the non-overcompressive subset of region V in cases 1–4. More detailed analysis of regions where we expect a combination of a delta-shock and classical solutions will be the subject of future work.

6. Numerical evidence on the various regions

Certain additional restrictions were placed on the numerical constants for the LLF method. We discuss only A, η , and k here, as β has minimal effect on qualitative behavior.

The magnitude of A is directly related to the size of the regions. We chose $|A| \ge 10$. Note that for large values of A, some regions become difficult to access numerically. Due to the e^{kt} term present in C_2 and R_2 , the parameter k controls the rate at which the curves change in time and therefore the regions. In this work, we chose |k| = 0.01 or $|k| \ge 0.6$. The former leads to curves that undergo minimal change in time, allowing insight into the initial combinations to enter regions. The latter approximates long-term behavior in time, modeling regional shift over time. While η alone does not have a strong effect on region behavior, we require $\eta - k > 0$ due to the factor of $e^{(\eta - k)t}$ in λ_1 and λ_2 . If $\eta - k < 0$, $\lim_{t \to \infty} e^{(\eta - k)t} = 0$, causing $\lambda_1 = \lambda_2$ in infinite time. We would then lose strict hyperbolicity of our regions, which is incompatible with our implementation and leads to unexpected results. Here, we present the numerical evidence for how the Riemann problem is solved for four cases involving a given left state and a right state in various regions. For case 1, region VIII, refer back to Fig. 3. We do not show region VIII (cases 1 and 3) and region II (cases 2 and 4) here, which is reached by R_2C_2 , since picking an appropriate point is difficult due to the difference between R_2 and C_2 being extremely small. We identify S_1 by its steep slope and lack of movement in w. R_2 is classified by a more gradual slope in combination with a "fanning" effect over all iterations. C_2 has some characteristics of both, often displaying a more gradual slope but with a consistent lack of fanning.

B. $\eta = k$ case

1. Hyperbolicity, linear degeneracy, and genuine nonlinearity

Equation (2.2) can be rewritten as

$$H_t + G_x = 0,$$
 (3.28)

where G and H are taken to be

$$\begin{cases}
H = \begin{bmatrix} v \\ vw \end{bmatrix}, \\
G = \begin{bmatrix} v(w + \beta t) - A(ve^{kt})^{\gamma+1} \\ vw(w + \beta t) - Aw(ve^{kt})^{\gamma+1} \end{bmatrix}.
\end{cases} (3.29)$$

To check, once again, whether our system is hyperbolic, $\det(DG - \lambda DH) = 0$ is solved, to find the eigenvalues

$$\begin{cases} \lambda_1 = (w + \beta t) - A(\gamma + 1)v^{\gamma}e^{kt(\gamma + 1)}, \\ \lambda_2 = (w + \beta t) - Av^{\gamma}e^{kt(\gamma + 1)}, \end{cases}$$
(3.30)

with the corresponding eigenvectors

≥ 2.5

4000

4000

Case 1: γ =-2 States *v*, *w*: 20000 Steps, t = 2.7204

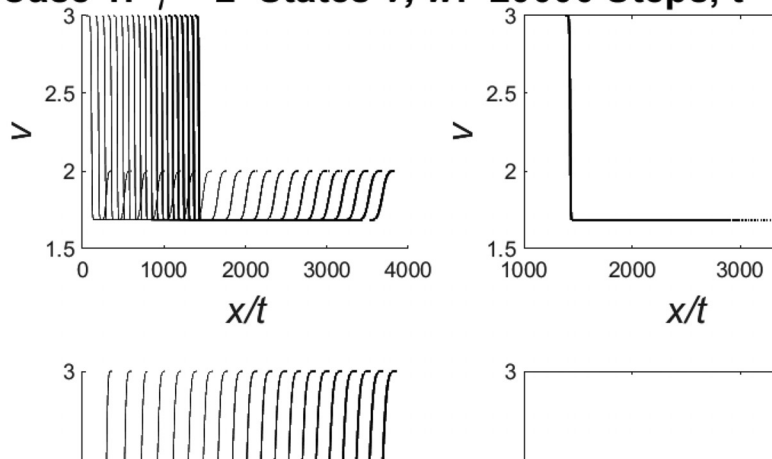


FIG. 8. Region VI of case 1, S_1C_2 . Parameters: $\gamma = -2, A = -10, \eta = 3, k = 0.01, \beta = 10.$

FIG. 9. Region VII of case 3, S_1C_2 .

Parameters: $\gamma = -2, A = -10, \eta = 3,$

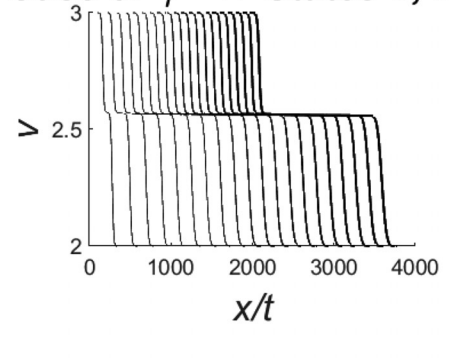
 $k = -0.01, \beta = 10.$

x/t; Data $U_L = (3,2), U_R = (2,3)$ x/t; Data $U_L = (3,2), U_R = (2,3)$ Case 3: γ =-2 States *v*, *w*: 20000 Steps, t = 2.7855

4000

≥ 2.5

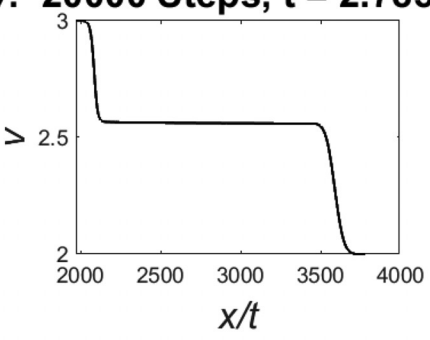
1000



2000

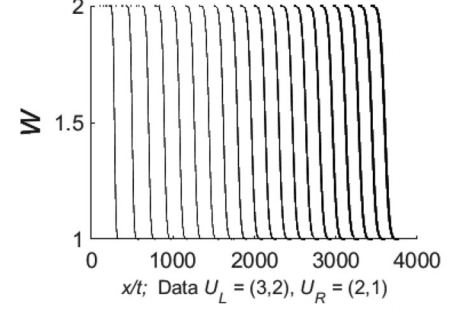
1000

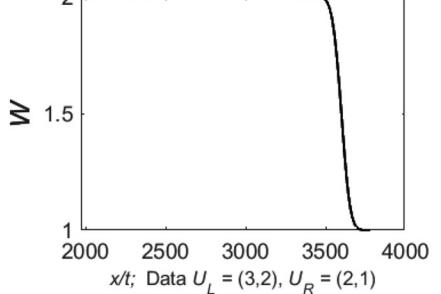
3000



2000

3000

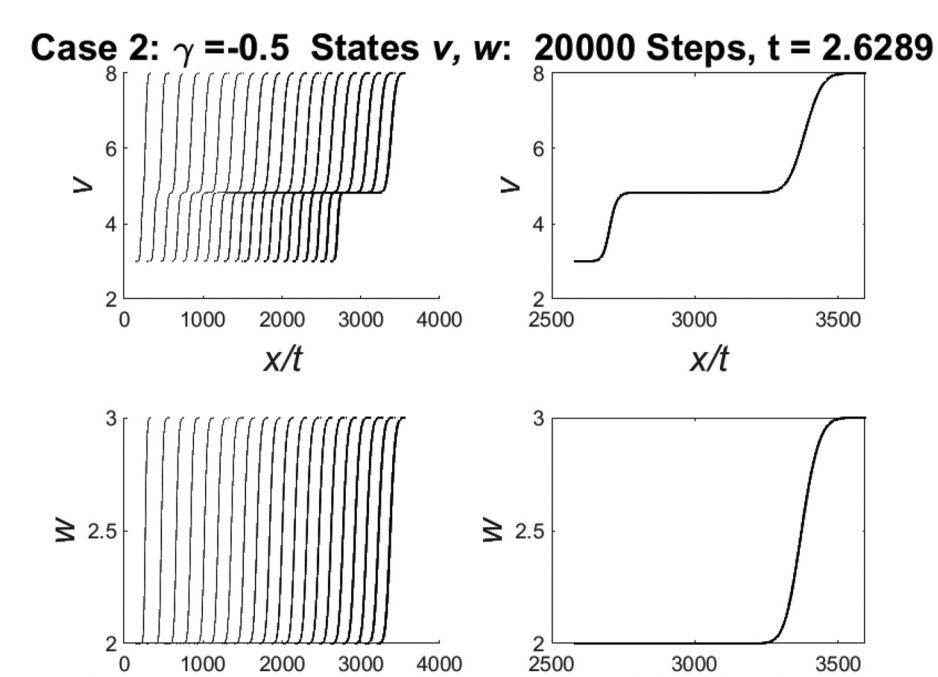




$$\left\{egin{aligned} r_1 &= egin{bmatrix} 1 \ 0 \end{bmatrix}, \ r_2 &= egin{bmatrix} 1 \ A \gamma v^{\gamma-1} e^{kt(\gamma+1)} \end{bmatrix}. \end{aligned}
ight.$$

(3.31)

Additionally,
$$\begin{cases} D\lambda_1 \cdot r_1 = -A\gamma(\gamma+1)v^{\gamma-1}e^{kt(\gamma+1)} \neq 0, \\ D\lambda_2 \cdot r_2 = -A\gamma v^{\gamma}e^{kt(\gamma+1)} + A\gamma v^{\gamma-1}e^{kt(\gamma+1)} = 0. \end{cases}$$
(3.32)



x/t; Data $U_L = (3,2), U_R = (8,3)$

x/t; Data $U_L = (3,2), U_R = (8,3)$

FIG. 10. Region III of case 2, S_1C_2 . Parameters: $\gamma=-0.5, A=-10, \eta=3, k=-0.01, \beta=10.$

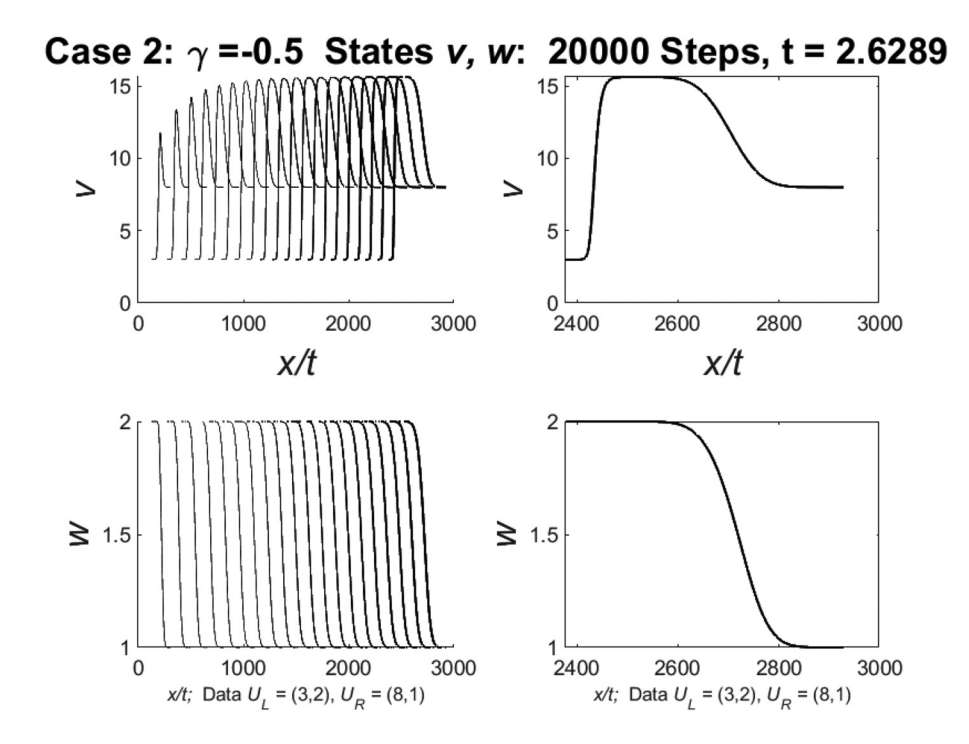


FIG. 11. Region IV of case 2, S_1C_2 . Parameters: $\gamma=-0.5, A=-10, \eta=3,$ $k=-0.01, \beta=10.$

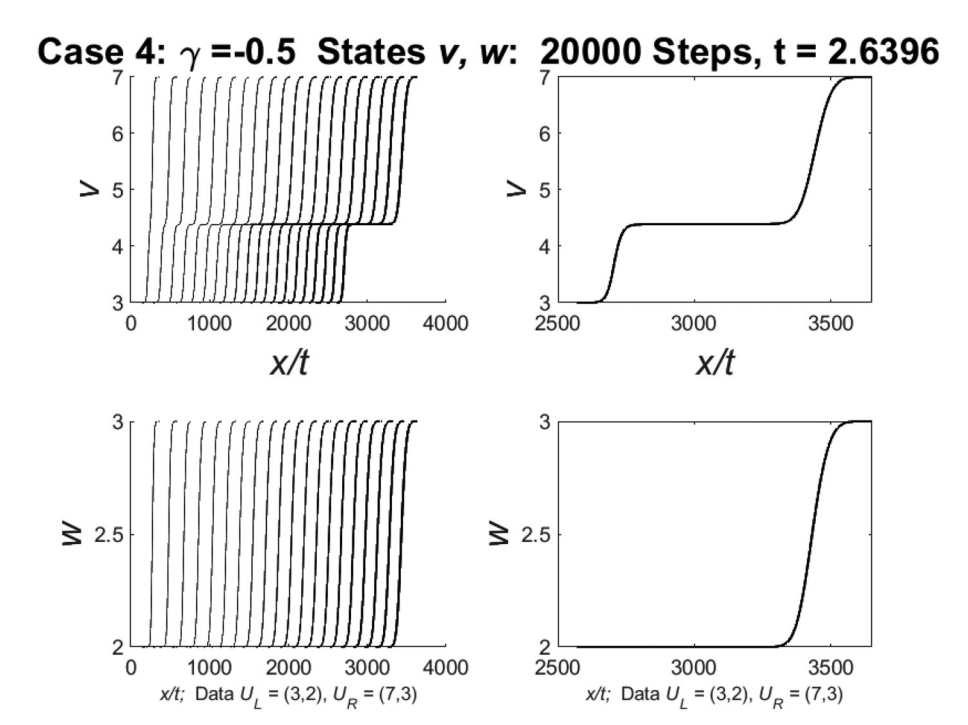


FIG. 12. Region III of case 4, S_1C_2 . Parameters: $\gamma=-0.5, A=-10, \eta=3, k=0.01, \beta=10.$

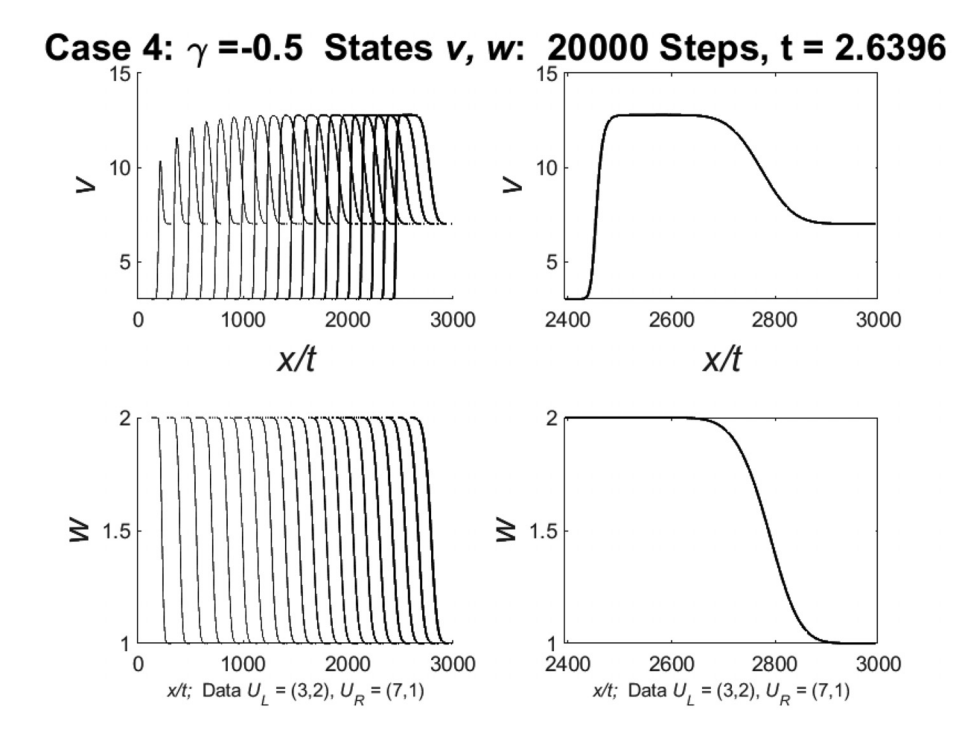


FIG. 13. Region IV of case 4, S_1C_2 . Parameters: $\gamma=-0.5, A=-10, \eta=3,$ $k=0.01, \beta=10.$

1000

2000

x/t; Data $U_L = (3,2), U_R = (1.5,1)$

3000

Case 1: γ =-2 States *v*, *w*: 20000 Steps, t = 2.7241

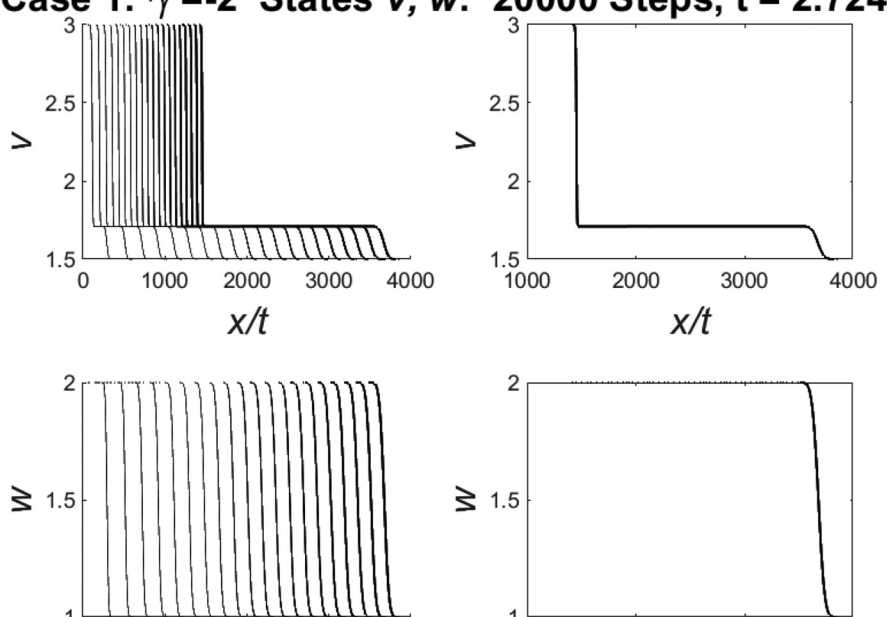


FIG. 14. Region VII of case 1, S_1R_2 . Parameters: $\gamma=-2, A=-10, \eta=3, k=0.01, \beta=10.$

Case 3: γ =-2 States *v*, *w*: 20000 Steps, t = 2.7008

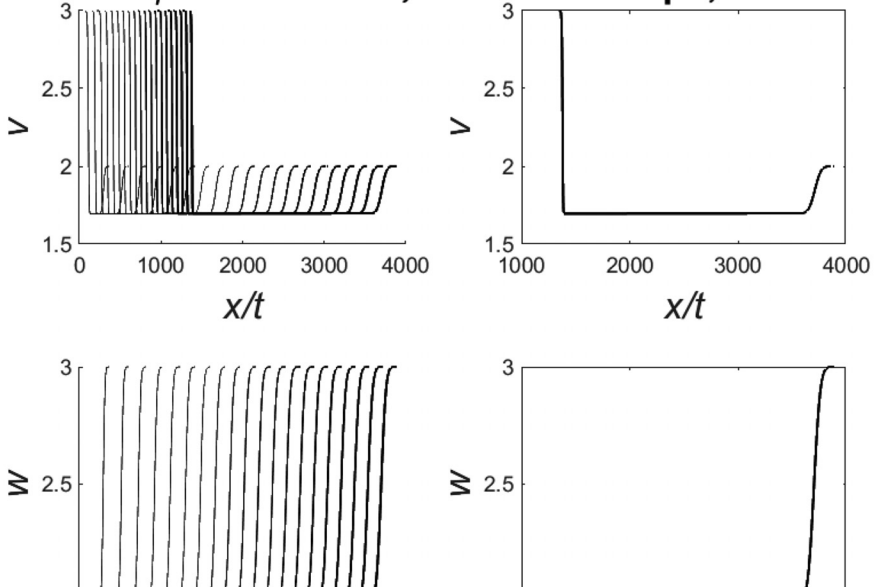
1000

2000

3000

x/t; Data $U_L = (3,2), U_R = (1.5,1)$

4000



1000

2000

x/t; Data $U_L = (3,2), U_R = (2,3)$

3000

4000

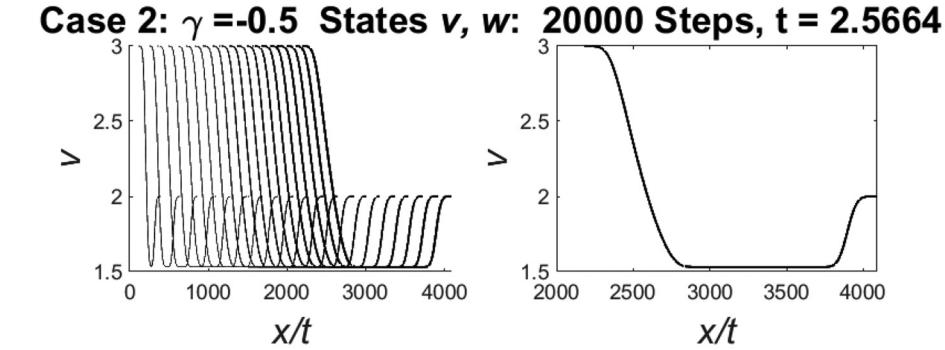
FIG. 15. Region VI of case 3, S_1R_2 . Parameters: $\gamma=-2, A=-10, \eta=3, k=-0.01, \beta=10.$

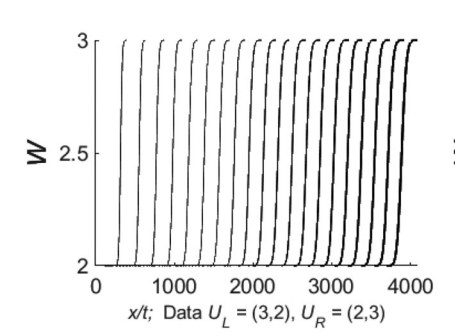
1000

2000

x/t; Data $U_L = (3,2), U_R = (2,3)$

4000





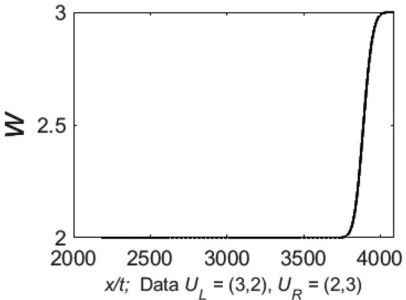
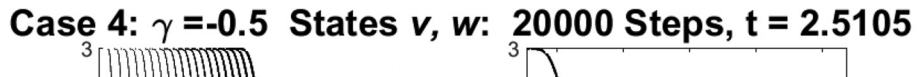
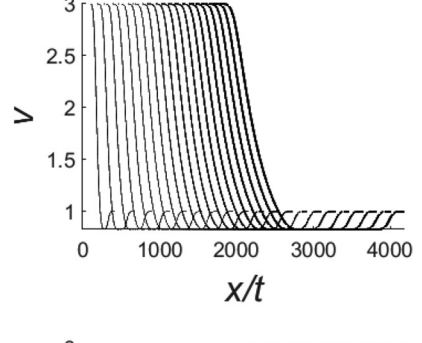
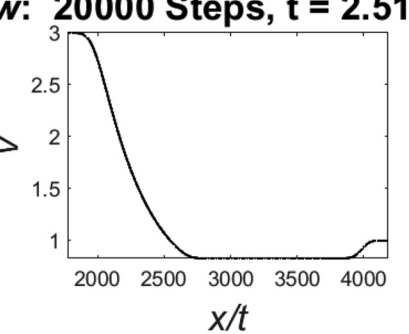
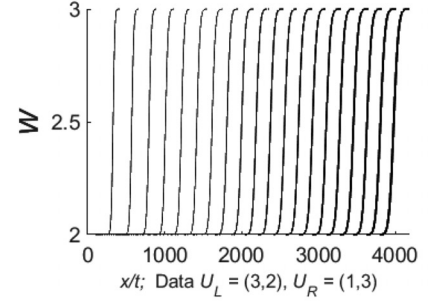


FIG. 16. Region I of case 2, R_2C_2 . Parameters: $\dot{\gamma} = -0.5, A = -10, \eta = 3,$ $k = -0.01, \dot{\beta} = 10.$









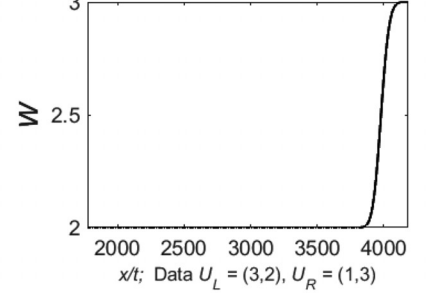


FIG. 17. Region I of case 4, R_2C_2 . Parameters: $\gamma = -0.5$, A = -10, $\eta = 3$, $k = 0.01, \beta = 10.$

Similar to the $\eta \neq k$ case, the one- and two-characteristic families are genuinely nonlinear and linearly degenerate, respectively.

2. Hugoniot locus through a left state (v_-,ω_-) : The Lax shock admissibility criterion

Once again, the Rankine–Hugoniot jump conditions (3.7) are checked and get

$$\begin{cases} -\sigma(t)[v]_{\text{jump}} + \left[v(w+\beta t) - A(ve^{kt})^{\gamma+1}\right]_{\text{jump}} = 0, \\ -\sigma(t)[vw]_{\text{jump}} + \left[vw(w+\beta t) - Aw(ve^{kt})^{\gamma+1}\right]_{\text{jump}} = 0, \end{cases}$$
(3.33)

resulting in

$$\begin{cases}
S_1(v_-, w_-) : w = w_-, \\
C_2(v_-, w_-) : w = w_- - \frac{A}{v_-} (v_- e^{kt})^{\gamma+1} + \frac{A}{v} (v_- e^{kt})^{\gamma+1}.
\end{cases}$$
(3.34)

Therefore, the states that can be connected to (v_-, w_-) by a one-shock or a two-contact discontinuity lie on the curves (3.34). By (3.33),

$$\sigma_1(t) = w_- + \beta t - A e^{kt(\gamma + 1)} \frac{v^{\gamma + 1} - v_-^{\gamma + 1}}{v - v_-}, \tag{3.35}$$

$$\sigma_2(t) = \lambda_2(v, w) = \lambda_2(v_-, w_-)$$
 (3.36)

are obtained. Again, (3.11) is checked to ensure that the Lax shock admissibility criterion is satisfied. The first and second inequalities give

$$v_{-}^{\gamma}(\gamma+1) > \frac{v_{-}^{\gamma+1} - v_{-}^{\gamma+1}}{v - v_{-}}$$
 (3.37)

and

$$v^{\gamma}(\gamma+1) < \frac{v^{\gamma+1} - v_{-}^{\gamma+1}}{v-v},$$
 (3.38)

respectively. Both are equivalent to the corresponding inequalities for the case $\eta \neq k$. Thus, S_1 exists for $v > v_-$ if $-1 < \gamma < 0$ and for $v < v_-$ if $\gamma < -1$. The rest of the analysis (non-existence of one-rarefactions, existence and location of two-rarefactions, regions, etc.) is identical to the $n \neq k$ case and will be omitted for brevity.

IV. DELTA-SHOCKS

In the overcompressibe subset of region V, there is no solution that is piecewise smooth, and bounded. Therefore, in order to establish existence in a space of measures from a mathematical perspective, a solution containing a weighted δ -measure (or δ -shock) supported on a curve needs to be constructed (see Refs. 30 and 31). For these singular solutions, we need to consider physical constraints. If w becomes unbounded, the system's velocity must approach infinity. However, this scenario is not physically possible, as we know that the speed of light bounds the velocity of all particles in the universe. Furthermore, it is also not physically feasible for both v and w to be unbounded, as it implies a finite amount of mass suddenly becoming infinite and then returning to a finite value. Therefore, the only possible case is for v to be unbounded. Assuming infinite density in situations where the fluid volume is nearly infinitesimal is physically reasonable. We have also

observed numerically the presence of the Dirac delta measure in ν only.

A. $\eta \neq k$ case

We define a two-dimensional weighted δ -measure $\omega(s)\delta_S$ supported on a smooth curve $S = \{(x(s), t(s)) : c \le s \le d\}$ by

$$\langle \omega(\cdot)\delta_{S}, \psi(\cdot, \cdot) \rangle = \int_{a}^{b} \omega(t(s))\psi(x(s), t(s)) ds$$

for all $\psi \in C_0^{\infty}(\mathbb{R} \times \mathbb{R}^+)$.

Following the above reasoning, the definition of solutions in the sense of distributions is as follows.

Definition: A pair (v, w) are known as a *delta-shock type solution* to the system with Riemann data in the sense of distributions if there exists a smooth curve $S = \{(x(t), t: 0 \le t < \infty)\}$ and a weight $\omega_1 \in C^1(S)$ such that v and w are represented in the following way

$$(v, w)(x, t) = (v_0(x, t) + \omega_1(t)\delta_S, w_0(x, t)),$$

$$= \begin{cases} (v_L, w_L), & x < x(t), \\ (v_\delta(t) + \omega_1(t)\delta(x - x(t)), w_\delta(t)), & x = x(t), \\ (v_R, w_R), & x > x(t), \end{cases}$$

$$(4.1)$$

where $\delta(\cdot)$ is the standard Dirac measure (therefore w is v-measurable, and for example, $v\left(w+\frac{\beta}{\eta-k}\right)$ can be understood as a Radon measure) and satisfy (2.1) in the sense of distributions:

$$\begin{split} \langle v, \phi_t \rangle + \left\langle v \left(w + \frac{\beta}{\eta - k} \right) e^{(\eta - k)t} - \frac{v\beta}{\eta - k} - A (v e^{kt})^{\gamma + 1} e^{(\eta - k)t}, \phi_x \right\rangle &= 0, \\ \left\langle v \left(w + \frac{\beta}{\eta - k} \right), \phi_t \right\rangle + \left\langle v \left(w + \frac{\beta}{\eta - k} \right)^2 e^{(\eta - k)t} \end{split}$$

$$(4.2)$$

$$-\left(w + \frac{\beta}{\eta - k}\right)e^{(\eta - k)t}A(ve^{kt})^{\gamma + 1} - \frac{\beta}{\eta - k}\left(w + \frac{\beta}{\eta - k}\right)v, \phi_x = 0,$$

$$(4.3)$$

for every $\phi \in C_0^{\infty}(\mathbb{R} \times \mathbb{R}^+)$, where

$$\begin{split} \langle v, \psi \rangle &= \int_0^\infty \int_{-\infty}^\infty v_0 \psi \, dx \, dt + \langle \omega_1(t) \delta_S, \psi \rangle, \\ \left\langle v \left(w + \frac{\beta}{\eta - k} \right), \psi \right\rangle &= \int_0^\infty \int_{-\infty}^\infty v_0 \left(w_0 + \frac{\beta}{\eta - k} \right) \psi \, dx \, dt \\ &+ \left\langle \omega_1(t) \left(w_\delta(t) + \frac{\beta}{\eta - k} \right) \delta_S, \psi \right\rangle, \\ \left\langle A(v e^{kt})^{\gamma + 1} e^{(\eta - k)t}, \psi \right\rangle &= \int_0^\infty \int_{-\infty}^\infty A(v_0 e^{kt})^{\gamma + 1} e^{(\eta - k)t} \psi \, dx \, dt, \end{split}$$

since γ < 0. The remaining integrals in (4.2) and (4.3) are similar. Therefore, (4.2) and (4.3) give

$$\int_{0}^{\infty} \int_{-\infty}^{x(t)} \left(v_{L} \phi_{t} + \left(v_{L} \left(w_{L} + \frac{\beta}{\eta - k} \right) e^{(\eta - k)t} - v_{L} \frac{\beta}{\eta - k} - A v_{L}^{\gamma + 1} e^{k(\gamma + 1)t} e^{(\eta - k)t} \right) \phi_{x} \right) dx dt
+ \int_{0}^{\infty} \int_{x(t)}^{\infty} \left(v_{R} \phi_{t} + \left(v_{R} \left(w_{R} + \frac{\beta}{\eta - k} \right) e^{(\eta - k)t} - v_{R} \frac{\beta}{\eta - k} - A v_{R}^{\gamma + 1} e^{k(\gamma + 1)t} e^{(\eta - k)t} \right) \phi_{x} \right) dx dt
+ \int_{0}^{\infty} \left(\omega_{1} \phi_{t} + \left(\omega_{1} \left(w_{\delta} + \frac{\beta}{\eta - k} \right) e^{(\eta - k)t} - \omega_{1} \frac{\beta}{\eta - k} \right) \phi_{x} \right) dt = 0$$
(4.4)

and

$$\int_{0}^{\infty} \int_{-\infty}^{x(t)} \left(v_{L} \left(w_{L} + \frac{\beta}{\eta - k} \right) \phi_{t} + \left(v_{L} \left(w_{L} + \frac{\beta}{\eta - k} \right)^{2} e^{(\eta - k)t} - \frac{\beta}{\eta - k} v_{L} \left(w_{L} + \frac{\beta}{\eta - k} \right) - A v_{L}^{\gamma + 1} e^{k(\gamma + 1)t} \left(w_{L} + \frac{\beta}{\eta - k} \right) e^{(\eta - k)t} \right) \phi_{x} \right) dxdt \\
+ \int_{0}^{\infty} \int_{x(t)}^{\infty} \left(v_{R} \left(w_{R} + \frac{\beta}{\eta - k} \right) \phi_{t} + \left(v_{R} \left(w_{R} + \frac{\beta}{\eta - k} \right)^{2} e^{(\eta - k)t} - \frac{\beta}{\eta - k} v_{R} \left(w_{R} + \frac{\beta}{\eta - k} \right) - A v_{R}^{\gamma + 1} e^{k(\gamma + 1)t} \left(w_{R} + \frac{\beta}{\eta - k} \right) e^{(\eta - k)t} \right) \phi_{x} \right) dxdt \\
+ \int_{0}^{\infty} \left(\omega_{1} \left(w_{\delta} + \frac{\beta}{\eta - k} \right) \phi_{t} + \left(\omega_{1} \left(w_{\delta} + \frac{\beta}{\eta - k} \right)^{2} e^{(\eta - k)t} - \frac{\beta}{\eta - k} \left(\omega_{1} \left(w_{\delta} + \frac{\beta}{\eta - k} \right) \right) \right) \phi_{x} \right) dt = 0, \tag{4.5}$$

respectively. To be able to integrate along x = x(t), we require

$$\frac{dx(t)}{dt} = \sigma(t) = \left(\omega_{\delta}(t) + \frac{\beta}{\eta - k}\right)e^{(\eta - k)t} - \frac{\beta}{\eta - k}.$$
(4.6)

We apply Green's Theorem, to write (4.4) and (4.5) as

$$\int_{0}^{\infty} \left(-[v]_{\text{jump}} \sigma + \left[v \left(w + \frac{\beta}{\eta - k} \right) e^{(\eta - k)t} - \frac{v\beta}{\eta - k} - A \left(v e^{kt} \right)^{\gamma + 1} e^{(\eta - k)t} \right]_{\text{jump}} - \frac{d\omega_{1}}{dt} \right) \phi dt = 0$$

$$(4.7)$$

and

$$\int_{0}^{\infty} \left(-\left[v \left(w + \frac{\beta}{\eta - k} \right) \right]_{\text{jump}} \sigma + \left[\left(w + \frac{\beta}{\eta - k} \right)^{2} v e^{(\eta - k)t} - \left(w + \frac{\beta}{\eta - k} \right) e^{(\eta - k)t} A (v e^{kt})^{\gamma + 1} - \frac{\beta}{\eta - k} \left(w + \frac{\beta}{\eta - k} \right) v \right]_{\text{jump}} - \frac{d}{dt} \left(\omega_{1} \left(\omega_{\delta} + \frac{\beta}{\eta - k} \right) \right) \phi dt = 0,$$
(4.8)

where $[\cdot]_{\text{jump}} = \cdot_L - \cdot_R$. Thus, if we also require

$$\frac{d\omega_1}{dt} = -[v]_{\text{jump}}\sigma + \left[v\left(w + \frac{\beta}{\eta - k}\right)e^{(\eta - k)t} - \frac{v\beta}{\eta - k} - A(ve^{kt})^{\gamma + 1}e^{(\eta - k)t}\right]_{\text{jump}}$$
(4.9)

$$\frac{d}{dt}\left(\omega_{1}\left(\omega_{\delta}+\frac{\beta}{\eta-k}\right)\right) = -\left[v\left(w+\frac{\beta}{\eta-k}\right)\right]_{\text{jump}}\sigma + \left[\left(w+\frac{\beta}{\eta-k}\right)^{2}ve^{(\eta-k)t} - \left(w+\frac{\beta}{\eta-k}\right)e^{(\eta-k)t}A(ve^{kt})^{\gamma+1} - \frac{\beta}{\eta-k}\left(w+\frac{\beta}{\eta-k}\right)v\right]_{\text{jump}},\tag{4.10}$$

then (v, w) satisfies the system in the sense of distributions, that is (4.2) and (4.3) hold for every test function ϕ . It should be noted that there is a Rankine–Hugoniot deficit in both components due to (4.9) and (4.10), just like in the chromatography model by Mazzotti *et al.*^{20–22} To get more information about ω_1 , w_δ and x(t) [with x(0) = 0, $\omega_1(0) = 0$], we return to the original variables $\rho_L(=v_L)$, $\rho_R(=v_R)$, $u_L(=w_L)$, $u_R(=w_R)$, and substitute (4.6) into (4.9) to get

$$\frac{d\omega_{1}}{dt} = -w_{\delta}e^{(\eta - k)t}[\rho]_{\text{jump}} + e^{(\eta - k)t}[\rho u]_{\text{jump}} - A[v^{\gamma + 1}]_{\text{jump}}e^{(\eta - k)t}e^{kt(\gamma + 1)}.$$
(4.11)

We then substitute (4.11) into (4.10) to obtain

$$\frac{d}{dt}(\omega_1 \omega_\delta) = -w_\delta e^{(\eta - k)t} [\rho u]_{\text{jump}} + e^{(\eta - k)t} [\rho u^2]_{\text{jump}} - A[uv^{\gamma + 1}]_{\text{jump}} e^{(\eta - k)t} e^{kt(\gamma + 1)}. \tag{4.12}$$

Integration of (4.11) and (4.12) yields

$$\begin{cases} \omega_{1}(t) = -[\rho]_{\text{jump}} \int_{0}^{t} w_{\delta}(s)e^{(\eta-k)s} ds + [\rho u]_{\text{jump}} \int_{0}^{t} e^{(\eta-k)s} ds - A[v^{\gamma+1}]_{\text{jump}} \int_{0}^{t} e^{(\eta-k)s}e^{ks(\gamma+1)} ds, \\ \omega_{1}\omega_{\delta} = -[\rho u]_{\text{jump}} \int_{0}^{t} w_{\delta}(s)e^{(\eta-k)s} ds + [\rho u^{2}]_{\text{jump}} \int_{0}^{t} e^{(\eta-k)s} ds - A[uv^{\gamma+1}]_{\text{jump}} \int_{0}^{t} e^{(\eta-k)s}e^{ks(\gamma+1)} ds. \end{cases}$$

$$(4.13)$$

We multiply the first equation with w_{δ} , subtract it from the second, and let $g(t) = \int_0^t w_{\delta}(s)e^{(\eta-k)s} ds$ to determine

$$\begin{cases} (\rho_{L} - \rho_{R})g'(t)g(t) + g'(t) \left(A\left(\rho_{L}^{\gamma+1} - \rho_{R}^{\gamma+1}\right) \left(\frac{e^{(k(\gamma+1)+\eta-k)t} - 1}{k(\gamma+1) + \eta - k} \right) - (\rho_{L}u_{L} - \rho_{R}u_{R}) \left(\frac{e^{(\eta-k)t} - 1}{\eta - k} \right) \right) - g(t)(\rho_{L}u_{L} - \rho_{R}u_{R})e^{(\eta-k)t} \\ + e^{(\eta-k)t} \left(\left(\rho_{L}u_{L}^{2} - \rho_{R}u_{R}^{2} \right) \left(\frac{e^{(\eta-k)t} - 1}{\eta - k} \right) - \left(Au_{L}\rho_{L}^{\gamma+1} - Au_{R}\rho_{R}^{\gamma+1} \right) \left(\frac{e^{(k(\gamma+1)+\eta-k)t} - 1}{k(\gamma+1) + \eta - k} \right) \right) = 0, \quad \text{when } \eta \neq -k\gamma, \\ (\rho_{L} - \rho_{R})g'(t)g(t) + g'(t) \left(A\left(\rho_{L}^{\gamma+1} - \rho_{R}^{\gamma+1}\right)t - (\rho_{L}u_{L} - \rho_{R}u_{R}) \left(\frac{e^{(\eta-k)t} - 1}{\eta - k} \right) \right) - g(t)(\rho_{L}u_{L} - \rho_{R}u_{R})e^{(\eta-k)t} \\ + e^{(\eta-k)t} \left(\left(\rho_{L}u_{L}^{2} - \rho_{R}u_{R}^{2} \right) \left(\frac{e^{(\eta-k)t} - 1}{\eta - k} \right) - \left(Au_{L}\rho_{L}^{\gamma+1} - Au_{R}\rho_{R}^{\gamma+1} \right)t \right) = 0, \quad \text{when } \eta = -k\gamma. \end{cases}$$

• When $\eta \neq -\gamma k, \gamma \neq -1$, and $\rho_L = \rho_R$, the solution of the first ODE in (4.14) is

$$\omega_{\delta} = \frac{-2A\rho_{L}^{\gamma}(k-\eta)e^{t((\gamma+2)k-\eta)} + (k\gamma+\eta)(u_{L}+u_{R})e^{2(k-\eta)t} - 2(u_{L}+u_{R})e^{(k-\eta)t} + \frac{1}{2}(u_{L}+u_{R})}{2(e^{(k-\eta)t}-1)^{2}} + \frac{-2A(k-\eta)^{2}\rho_{L}^{\gamma}e^{2(k-\eta)t} + A(k-\eta)\rho_{L}^{\gamma}e^{kt(\gamma+1)}}{2((\gamma-1)k+2\eta)(e^{(\eta-k)t}-1)^{2}}.$$

$$(4.15)$$

• When $\eta=-\gamma k, \gamma \neq -1$, and $\rho_L=\rho_R$, the solution of the second ODE in (4.14) is

$$\omega_{\delta} = \frac{1}{\left(e^{(k-\eta)t} - 1\right)^2} \left(\left((1 + (\eta - k)t)A\rho_L^{\gamma} - u_L - u_R \right) e^{-2(\eta - k)t} - \left(A\rho_L^{\gamma} + u_L + u_R \right) e^{(k-\eta)t} + u_L + u_R \right). \tag{4.16}$$

We note that when $\rho_L \neq \rho_R$, the ODEs cannot be solved explicitly. Figure 18 is an example obtained numerically when $\eta = -k\gamma$ with parameters $A = -10, \gamma = -4, k = 1, \eta = 4, \beta = 2, \rho_L = 2, u_L = 3, u_R = 2, \rho_R = 4$. A similar graph (although it might be flipped across the *t*-axis) is obtained for other parameters as well as for when $\eta \neq -k\gamma$.

1. Overcompressible region

We seek delta-shocks connecting a given left state (v_-, w_+) with a right state (v, w) that are overcompressive, meaning that all characteristic curves run into the delta-shock curve from both sides. Therefore, we require the following inequality:

$$\lambda_1(v, w) < \lambda_2(v, w) \le \frac{dx(t)}{dt} \le \lambda_1(v_-, w_-) < \lambda_2(v_-, w_-).$$
 (4.17)

The outer inequalities always hold. Note, ω_{δ} generally cannot be solved explicitly. Thus, we consider $\lambda_2(v,w) < \lambda_1(v_-,w_-)$ to locate the region that would contain the right states that result in a strictly overcompressive delta-shock. This inequality indicates an upper border

$$J: w = w_{-} - A(\gamma + 1)v_{-}^{\gamma}e^{kt(\gamma + 1)} + Av^{\gamma}e^{kt(\gamma + 1)}.$$
 (4.18)

After some simplification, this curve is the same in the $\eta = k$ case. Hence, it yields the same region. *J* is above S_{δ} , given by (3.25), when $-1 < \gamma < 0$ and below when $\gamma < -1$. As mentioned above, Dirac delta functions are observed numerically only in ν , as shown in Fig. 19.

2. Region shift for $k(\gamma + 1) < 0$

In this case, as $t \to \infty$, the C_2 and R_2 curves converge to $w = w_L$ with C_2 maintaining an asymptote at v = 0. This allows for a point in a given region to shift to another as time progresses. The behavior of regions is found to progress as shown in Figs. 20 and 21. In addition, as time approaches infinity, (3.25) and (4.18) will approach $w = w_L$. Therefore, the set of overcompressible points will be a subset of region V in Fig. 20. The solutions to the Riemann problem will consist of

- A one-shock followed by a two-contact discontinuity when the right state is in region VI (see Fig. 22)
- A one-shock followed by a two-rarefaction when the right state is in region VII
- An overcompressive delta-shock or a combination of a delta-shock and a classical wave when the right state is in region V (see Fig. 23)

The limit will affect case 2 in a similar way: However, we now expect that

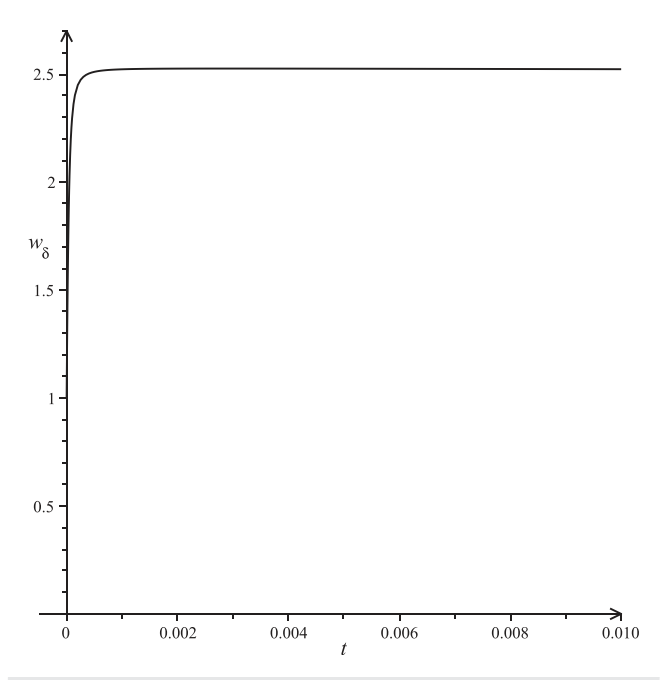


FIG. 18. Numerical solution for ω_{δ} when $\eta = -k\gamma$.

- A two-rarefaction followed by a two-contact discontinuity when the right state is in region I (see Fig. 24)
- An overcompressive delta-shock or a combination of a deltashock and a classical wave when the right state is in region V

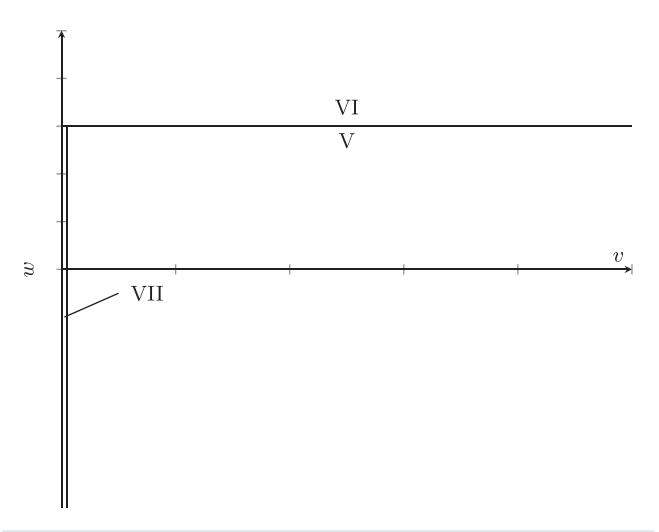


FIG. 20. Limit behavior of the regions for $\gamma < -1$ and k > 0.

An example of how a solution changes as time progresses when a right state is initially in region II of case 2 is given in Fig. 25.

3. Region shift for $k(\gamma + 1) > 0$

As $t \to \infty$, the shift of the regions will require more careful consideration since

$$\lim_{t\to\infty}\left(w_- + \frac{A}{v}(ve^{kt})^{\gamma+1}\right) = -\infty. \tag{4.19}$$

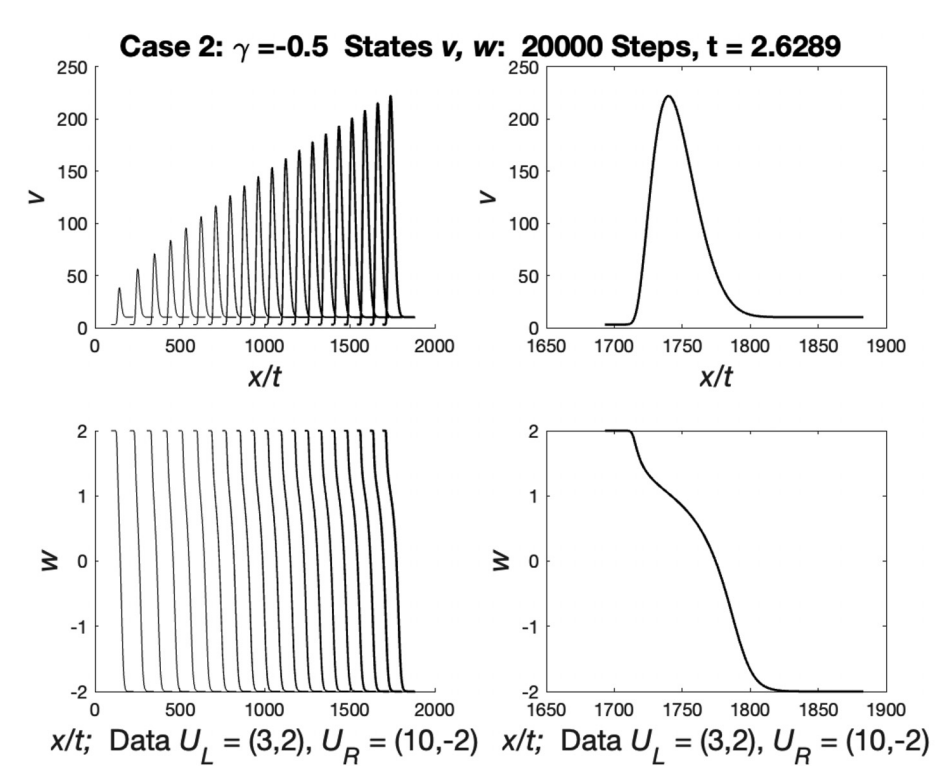


FIG. 19. Region V in Fig. 5. Dirac delta function in region V. Parameters: $\gamma = -0.5, A = -10, \eta = 3, k = -0.01, \beta = 10.$

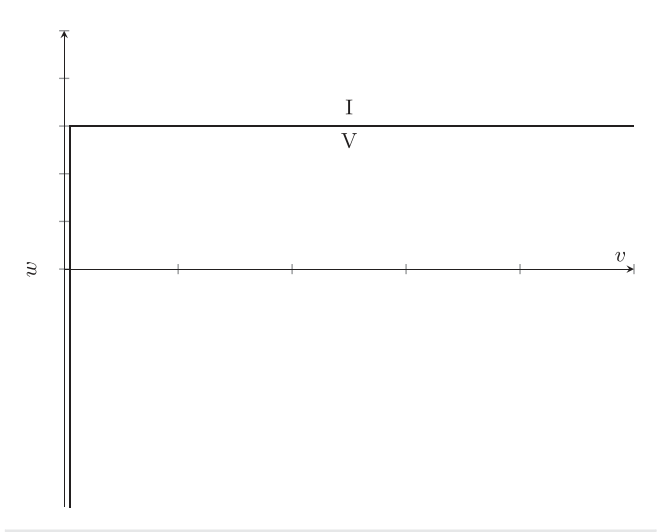


FIG. 21. Limit behavior of the regions for $-1 < \gamma < 0$ and k < 0.

Therefore, S_{δ} moves farther down in the plane (when $\gamma < -1$ the overcompressive region moves in the same spirit because it is located below S_{δ}). Next, we check the time behavior of C_2 . Since

$$\lim_{t \to \infty} \left(w_- + \frac{A}{v} (v e^{kt})^{\gamma + 1} - \frac{A}{v_-} (v_- e^{kt})^{\gamma + 1} \right)$$

$$= \lim_{t \to \infty} \left(w_- + A (v^{\gamma} - v_-^{\gamma}) e^{kt(\gamma + 1)} \right) = \begin{cases} -\infty & \text{when } v < v_-, \\ +\infty & \text{when } v > v_-, \end{cases}$$

$$(4.20)$$

the regions will shift as shown in Figs. 26 and 27.

When $-1 < \gamma < 0$, the solutions to the Riemann problem will consist of

- A two-rarefaction followed by a two-contact discontinuity when the right state is in region I (see Fig. 28)
- A one-shock followed by a two-contact discontinuity when the right state is in regions III and IV (see Fig. 29)

The $\gamma<-1$ case has a similar transformation as seen below. In this final case, the solution will consist of

- A one-shock followed by a two-rarefaction when (ν_R, w_R) is in region VI (see Fig. 30). This means that R₂ remains above C₂ during the region shift.
- A one-shock followed by a two-contact discontinuity when (v_R, w_R) is in region VII (see Fig. 31)
- Either a delta-shock followed by a two-wave or a two-contact discontinuity followed by a delta-shock when the right state is in region IX. The set of overcompressible points will be a subset of region V in Fig. 27.

4. Non-overcompressive regions

Before region shift, solutions with right states in region IX, case 1, display combinations of a delta-shock and a classical solution. Between S_{δ} and S_{o} , a delta-shock is followed by a two-wave. This is supported by Fig. 32, as the two-wave in w only occurs after the initial delta-shock. Above S_{δ} , we observe a two-contact discontinuity followed by a delta-shock. Note that the diffusion in the first wave is likely due to the cell averaging involved in the LLF method as the delta-shock grows.

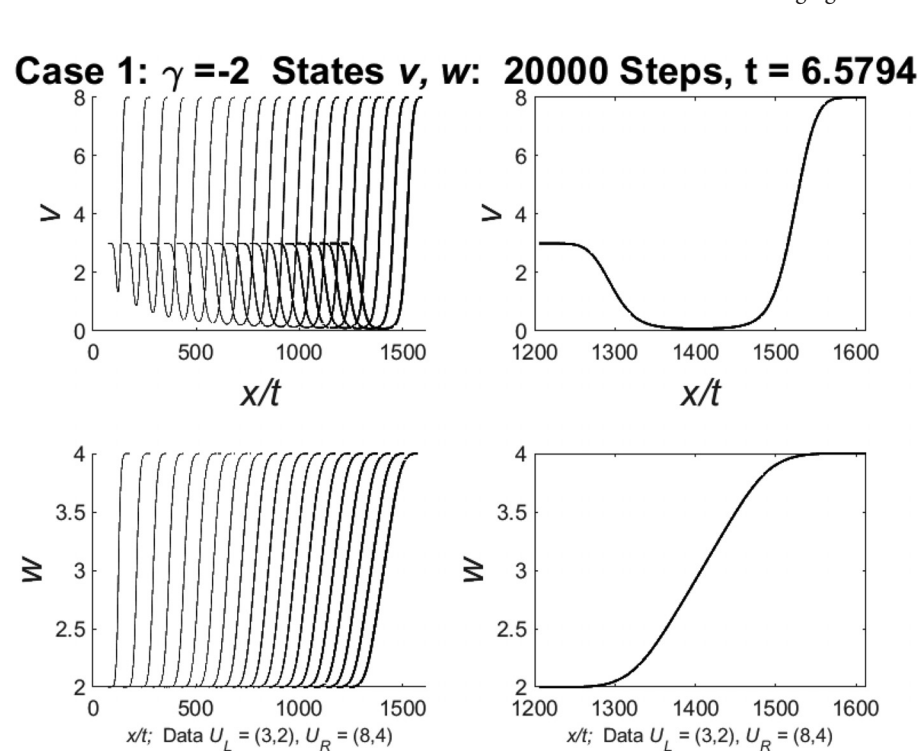
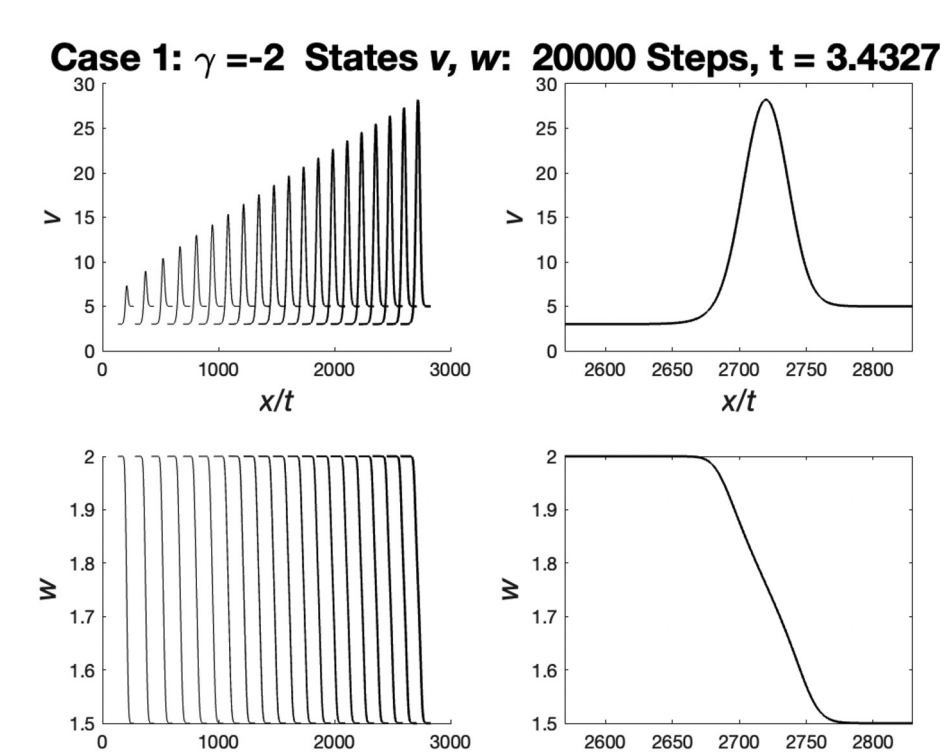


FIG. 22. Region VI of Fig. 20. Region shifts to S_1C_2 . Parameters: $\gamma=-2$, A=-10, $\eta=3$, k=2, $\beta=10$.

2750

x/t; Data $U_L = (3,2), U_R = (5,1.5)$

2800



x/t; Data $U_L = (3,2), U_R = (5,1.5)$

FIG. 23. Region V of Fig. 20. The region shifts to a delta-shock over time in v. Parameters: $\gamma = -2, A = -10, \eta = 3,$ $k = 0.6, \beta = 10.$

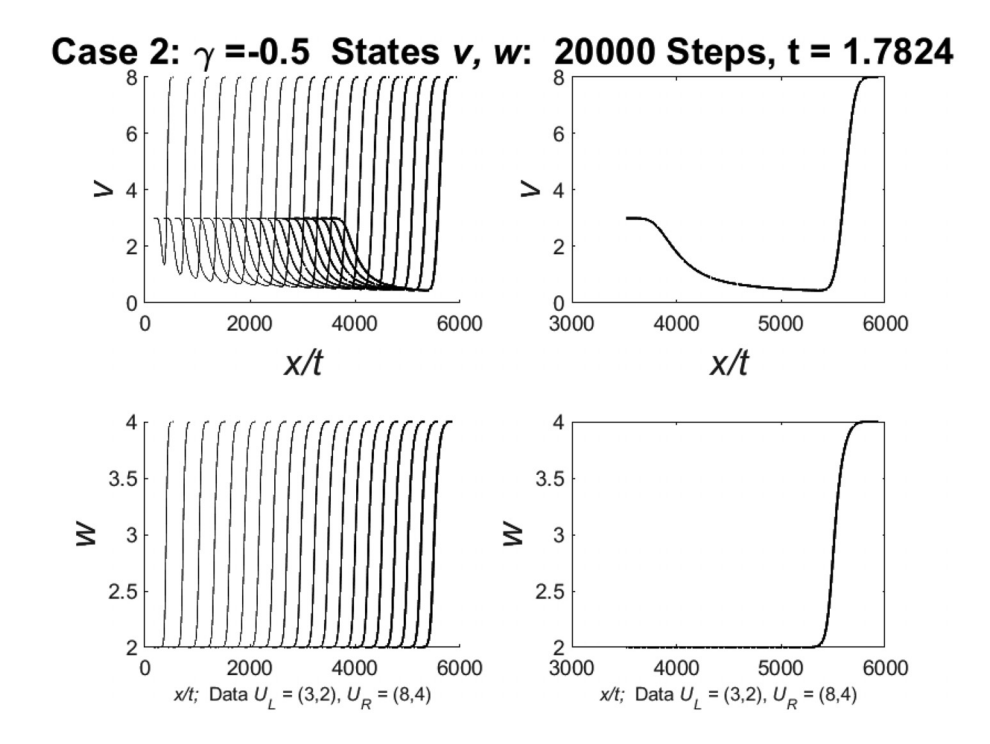


FIG. 24. Region I of Fig. 21. Region shifts $\text{to} \quad \textit{R}_2\textit{C}_2. \quad \text{Parameters:} \quad \gamma = -0.5,$ A = -10, $\eta = 3$, k = -2, $\beta = 10$.

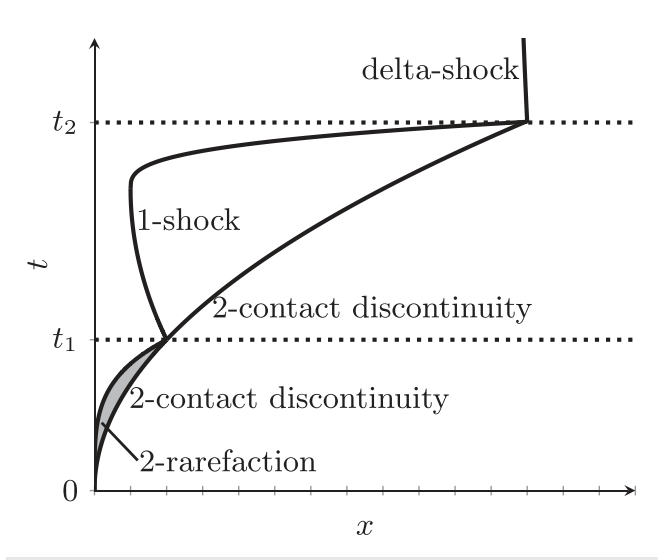


FIG. 25. An example solution for a (V_R, W_R) originally in region II case 2.

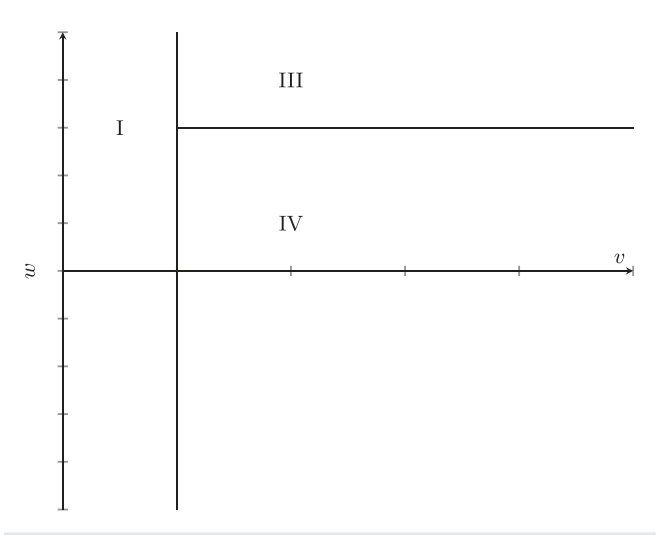


FIG. 26. Limit behavior of the regions for $-1 < \gamma < 0$ and k > 0.

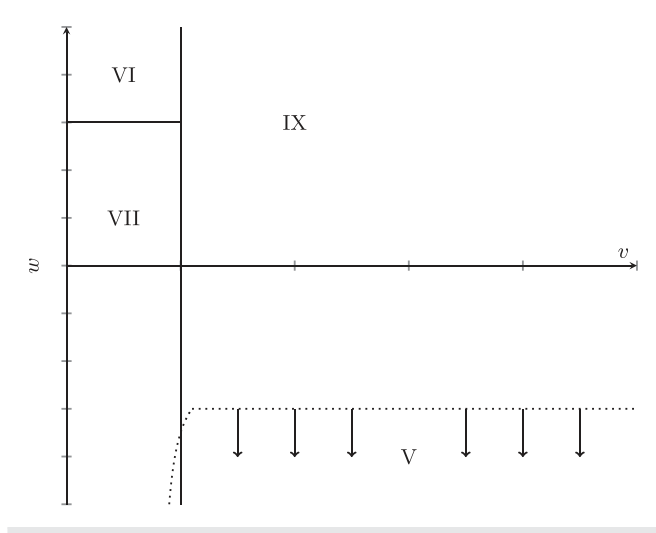


FIG. 27. Limit behavior of the regions for $\gamma < -1$ and k < 0.

Further testing with other numerical methods is needed to confirm this. We find that proximity to S_{δ} shows increased delta-shock characteristics numerically, while proximity to C_2 muddles those characteristics. We demonstrate this in Figs. 33 and 34. We propose this is due to the curve needing to travel farther along C_2 to a middle state, raising the overcompressive region, and allowing for a delta-shock to be taken. If this is the case, it would explain why numerically a proximity to the C_2 curve would cause an unclear delta characteristic as the curve must travel incredibly far in order to raise the overcompressive region a sufficient amount.

Note that in case 3, S_{δ} and S_{o} approach the same limit. Case 1 shares the same short term behavior of non-overcompressive delta regions, but it is lost upon region shift. This is shown in Figs. 35–38. As shown in Fig. 37, as overcompressibility disappears during region shift, the delta shock becomes much weaker.

B. $\eta = k$ case

We follow the delta-shock definition as before; therefore, our solution should satisfy the equations

$$\begin{split} \left\langle v,\phi_{t}\right\rangle + \left\langle v(w+\beta t) - A(ve^{kt})^{\gamma+1},\phi_{x}\right\rangle &= 0,\\ \left\langle vw,\phi_{t}\right\rangle + \left\langle v(w+\beta t)w - A(ve^{kt})^{\gamma+1}w,\phi_{x}\right\rangle &= 0, \end{split} \tag{4.21}$$

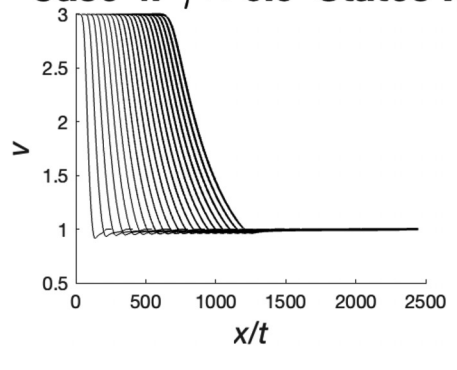
for any $\phi \in C_0^{\infty}(\mathbb{R} \times \mathbb{R}^+)$. We use the properties of the Dirac delta function in a similar manner to the $\eta \neq k$ case to observe that

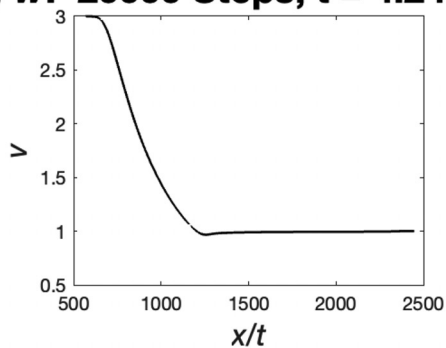
$$\langle v, \phi_{t} \rangle + \left\langle v(w + \beta t) - A(ve^{kt})^{\gamma+1}, \phi_{x} \right\rangle = \int_{0}^{\infty} \int_{-\infty}^{x(t)} v_{L} \phi_{t} dx dt + \int_{0}^{\infty} \int_{-\infty}^{x(t)} v_{L}(w_{L} + \beta t) \phi_{x} dx dt + \int_{0}^{\infty} \int_{x(t)}^{\infty} v_{R}(w_{R} + \beta t) \phi_{x} dx dt + \int_{0}^{\infty} \int_{x(t)}^{\infty} v_{R} \phi_{t} dx dt + \int_{0}^{\infty} (\omega_{1} \phi_{t} + \omega_{1}(w_{\delta} + \beta t) \phi_{x}) dt - \int_{0}^{\infty} \int_{-\infty}^{x(t)} A(v_{L} e^{kt})^{\gamma+1} \phi_{x} dx dt - \int_{0}^{\infty} \int_{x(t)}^{\infty} A(v_{R} e^{kt})^{\gamma+1} \phi_{x} dx dt$$

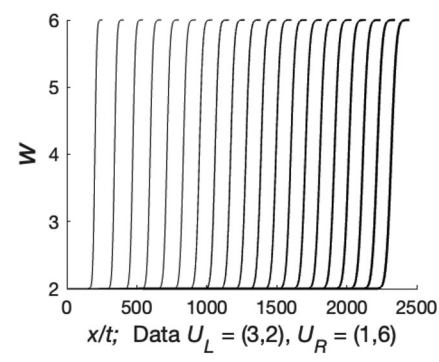
$$(4.22)$$

and

Case 4: γ =-0.5 States v, w: 20000 Steps, t = 4.24







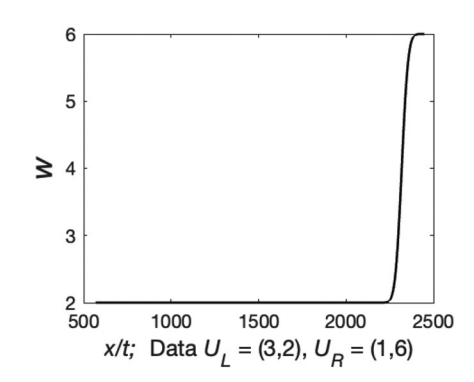
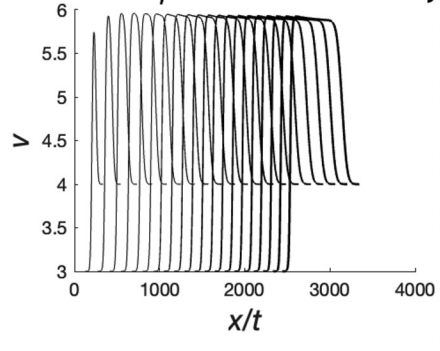
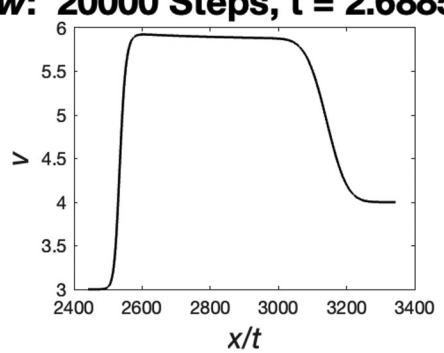
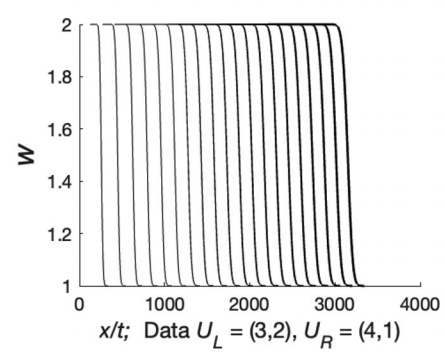


FIG. 28. Region I of Fig. 26. Region shifts to R_2C_2 in time. Parameters: $\gamma=-0.5$, A=-10, $\eta=3$, k=2.5, $\beta=10$.

Case 4: γ =-0.5 States *v*, *w*: 20000 Steps, t = 2.6885







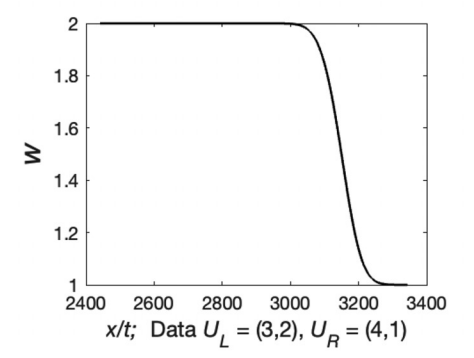
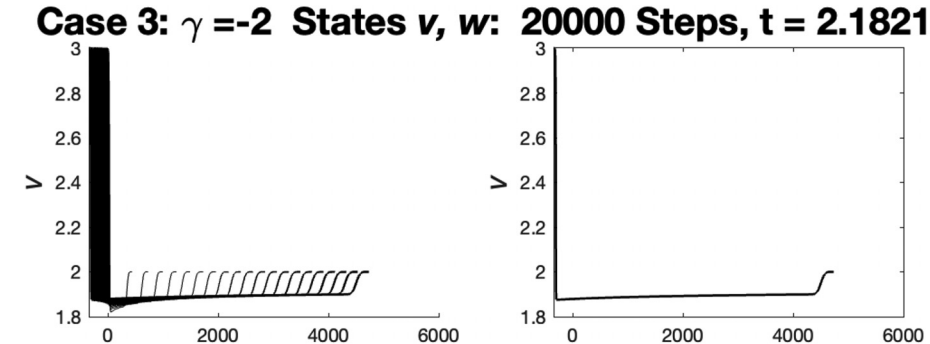
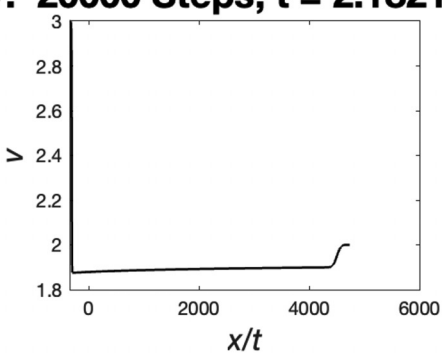
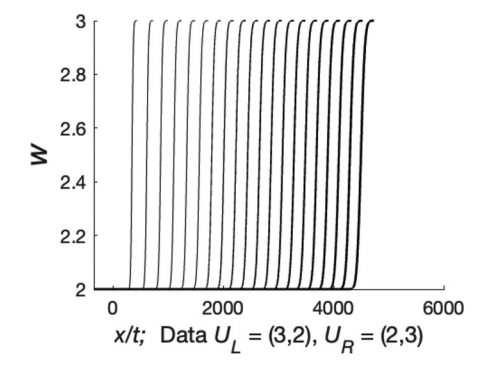


FIG. 29. Region III of Fig. 26. Region shifts to S_1C_2 in time. Parameters: $\gamma=-0.5$, A=-10, $\eta=3$, k=0.1, $\beta=10$.



x/t





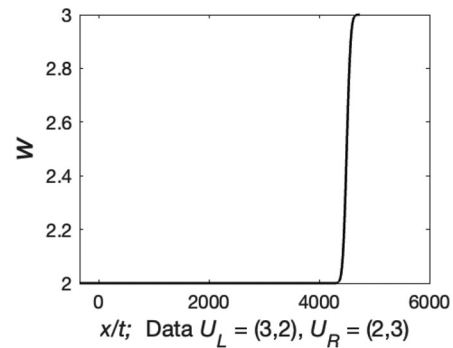
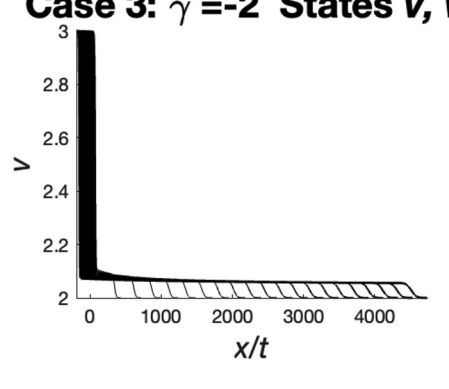
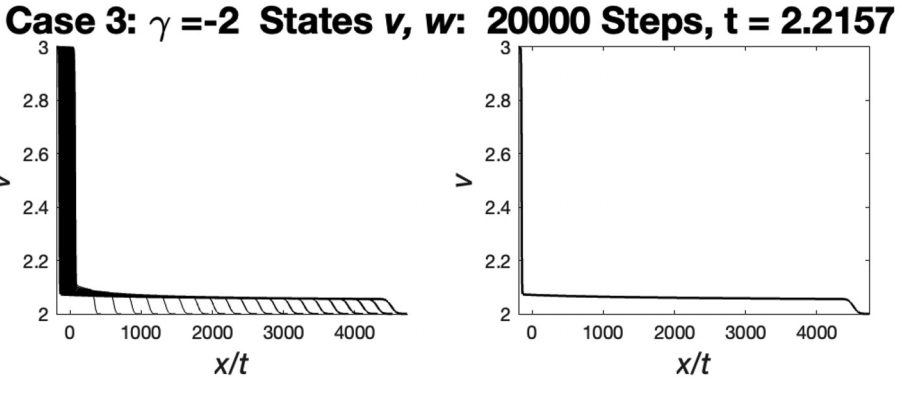
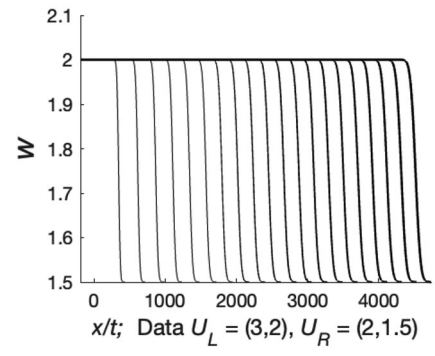


FIG. 30. Region VI of Fig. 27. Region shifts to S_1R_2 . Parameters: $\gamma = -2$, $A = -10, \eta = 3, k = -0.6, \beta = 10.$







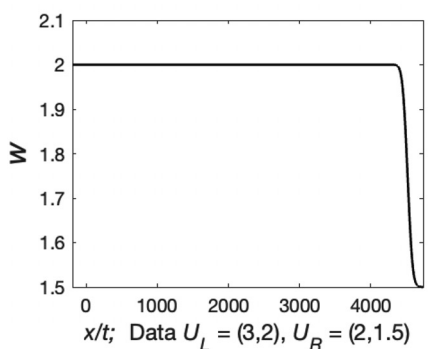
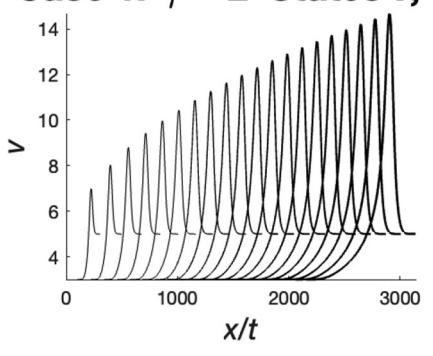
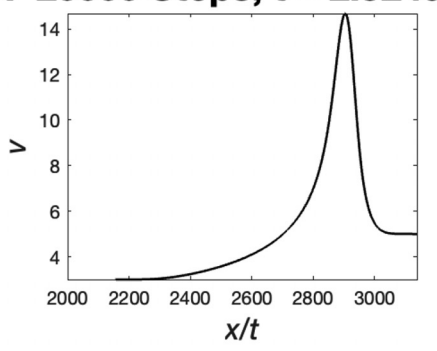
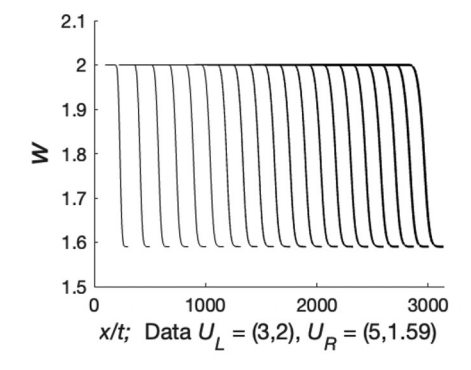


FIG. 31. Region VII in Fig. 27. Region shifts to S_1C_2 . Parameters: $\gamma = -2, A$ $=-10, \eta=3, k=-0.6, \beta=10.$

Case 1: γ =-2 States *v*, *w*: 20000 Steps, t = 2.8249







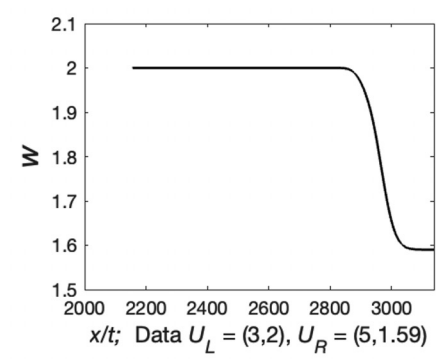
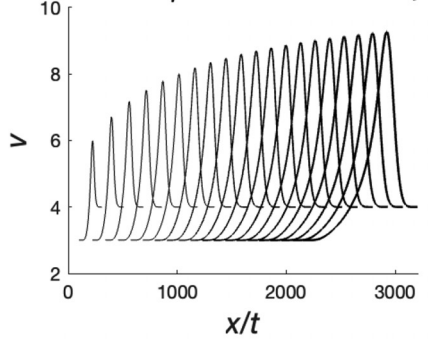
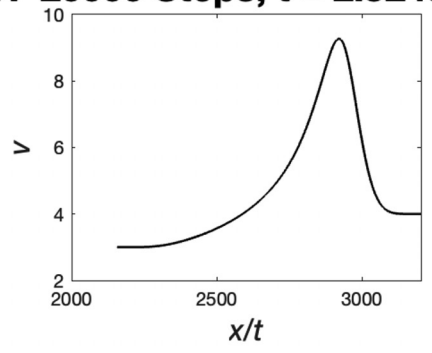
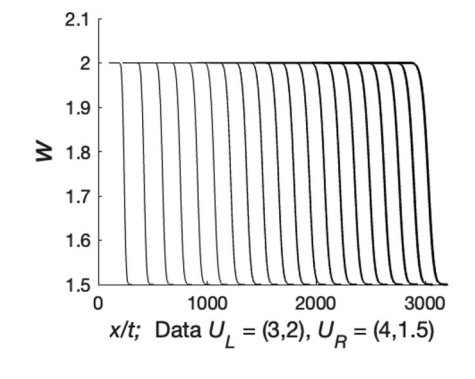


FIG. 32. Region IX of Fig. 4, δ 2-wave, between S_{δ} and S_{o} . Parameters: $\gamma=-2$, A=-10, $\eta=3$, k=0.01, $\beta=10$.

Case 1: γ =-2 States *v*, *w*: 20000 Steps, t = 2.8249







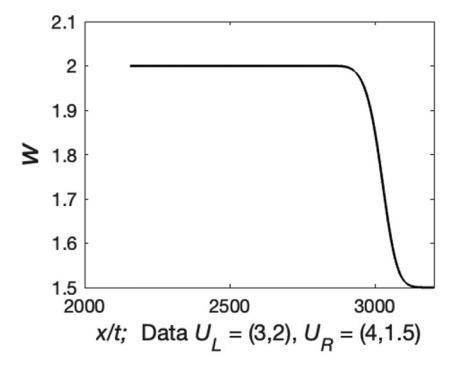


FIG. 33. Region IX of Fig. 4, $C_2\delta$, close to and above S_δ . Parameters: $\gamma=-2$, A=-10, $\eta=3$, k=0.01, $\beta=10$.

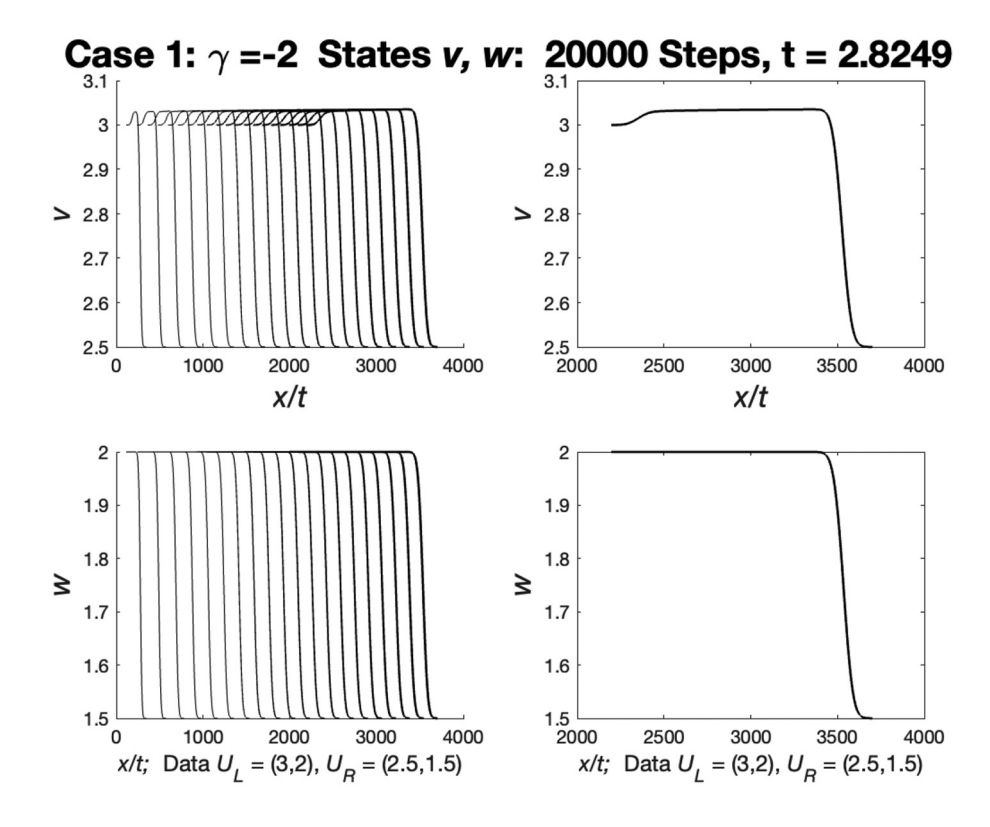


FIG. 34. Region IX of Fig. 4, $C_2\delta$, farther from and above S_δ . Parameters: $\gamma=-2$, A=-10, $\eta=3$, k=0.01, $\beta=10$.

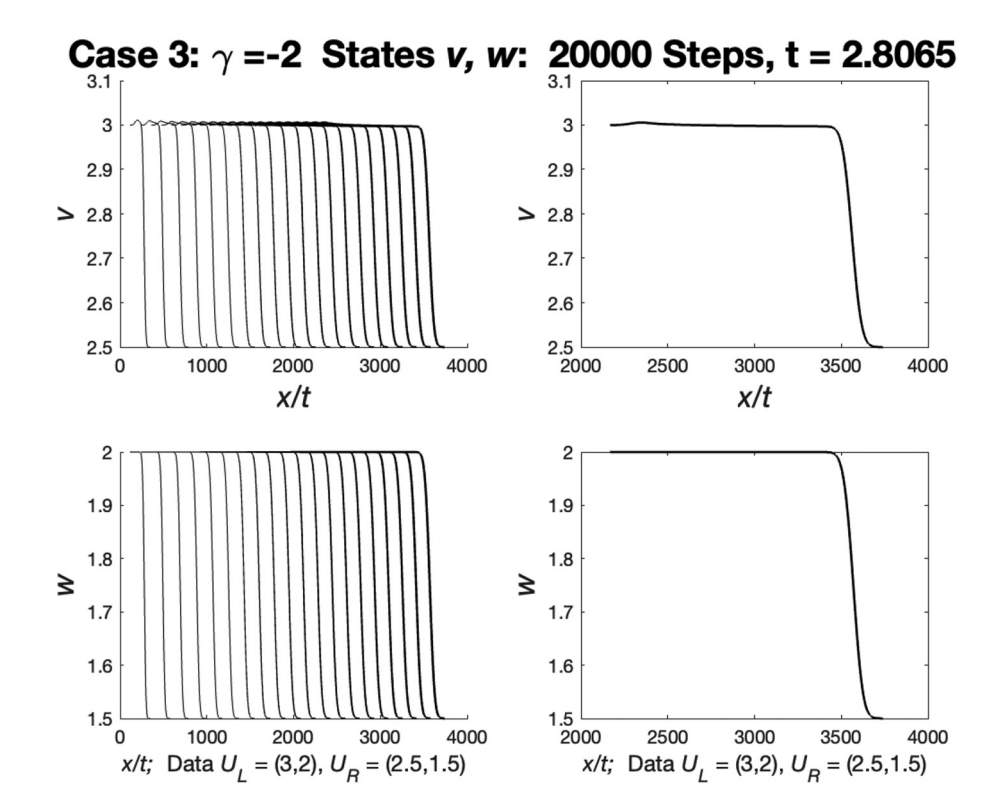


FIG. 35. Region IX of Fig. 6, $C_2\delta$, close to C_2 and above S_δ . Parameters: $\gamma=-2$, A=-10, $\eta=3$, k=-0.01, $\beta=10$.

1.6

1.5 ^{_}0

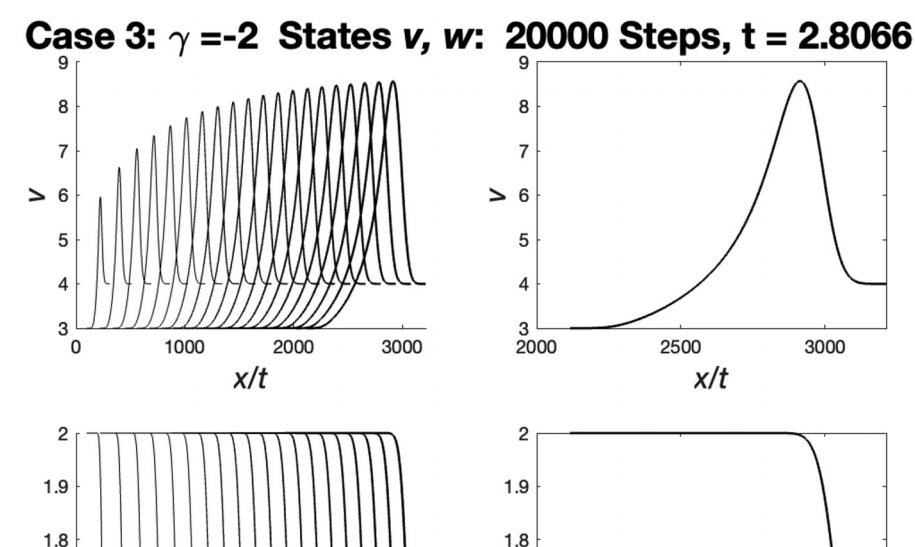
2.8

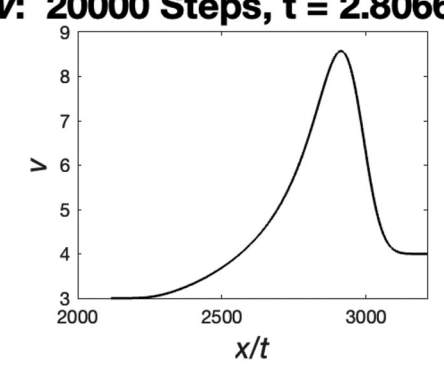
2.7

0

1000

1000





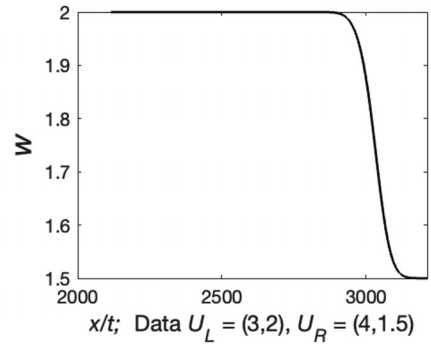


FIG. 36. Region IX of Fig. 6, $C_2\delta$, far from C₂ and above S_{δ}. Parameters: $\gamma = -2$, A = -10, $\eta = 3$, k = -0.01, $\beta = 10$.



3000

x/t

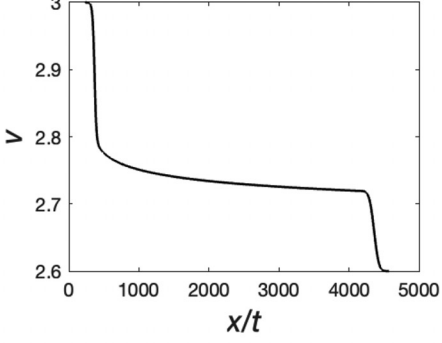
4000

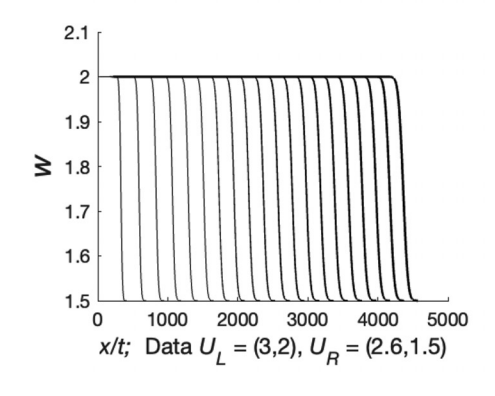
5000

Case 3: γ =-2 States *v*, *w*: 20000 Steps, t = 2.295

2000

x/t; Data $U_L = (3,2), U_R = (4,1.5)$





2000

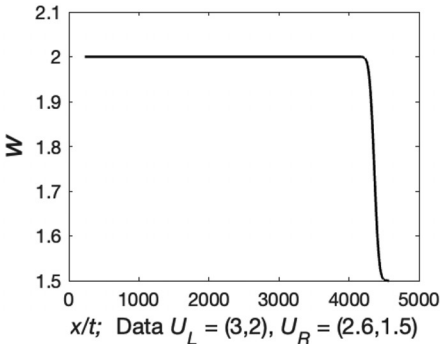
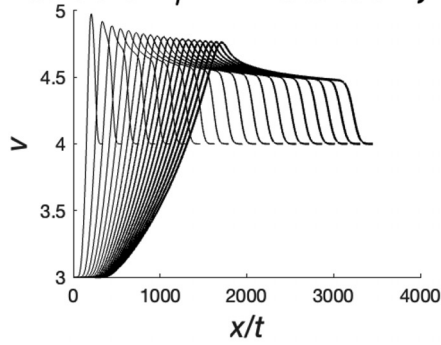
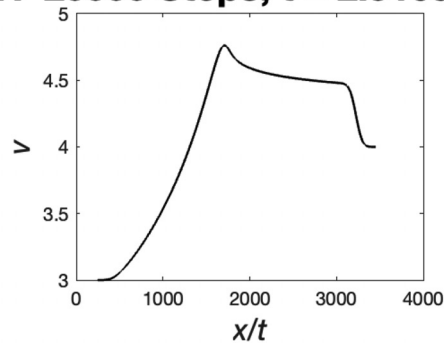
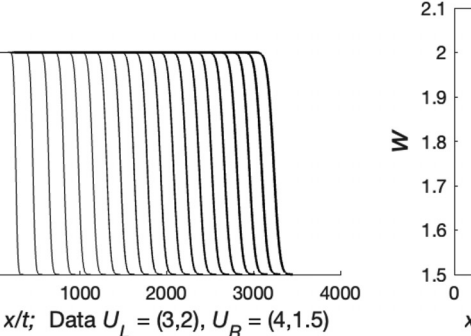


FIG. 37. Region IX of Fig. 27, $C_2\delta$, close to C₂ and above S_{δ}. Parameters: $\gamma = -A = -10$, $\eta = 3$, k = -0.6, $\beta = 10$.

Case 3: γ =-2 States *v*, *w*: 20000 Steps, t = 2.3168







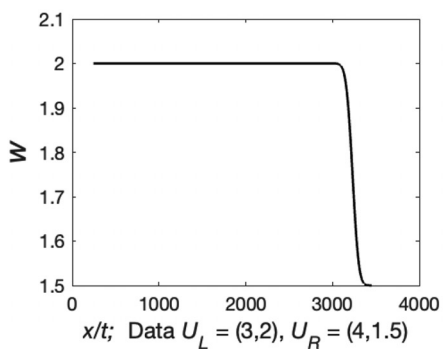


FIG. 38. Region IX of Fig. 27, $C_2\delta$, far from C_2 and above S_δ . Parameters: $\gamma=-2$, A=-10, $\eta=3$, k=-0.6, $\beta=10$.

$$\langle vw, \phi_t \rangle + \left\langle v(w + \beta t)w - A(ve^{kt})^{\gamma+1}w, \phi_x \right\rangle = \int_0^\infty \int_{-\infty}^{x(t)} v_L w_L \phi_t dx dt + \int_0^\infty \int_{-\infty}^{x(t)} v_L (w_L + \beta t) w_L \phi_x dx dt + \int_0^\infty \int_{x(t)}^\infty v_R (w_R + \beta t) w_R \phi_x dx dt + \int_0^\infty \int_{x(t)}^\infty v_R w_R \phi_t dx dt + \int_0^\infty (\omega_1 w_\delta \phi_t + \omega_1 (w_\delta + \beta t) w_\delta \phi_x) dt - \int_0^\infty \int_{-\infty}^{x(t)} A(v_L e^{kt})^{\gamma+1} w_L \phi_x dx dt - \int_0^\infty \int_{x(t)}^\infty A(v_R e^{kt})^{\gamma+1} w_R \phi_x dx dt.$$

$$(4.23)$$

We require

2.1

≥ 1.8

1.7 1.6

2

$$\frac{dx(t)}{dt} = \sigma(t) = \omega_{\delta}(t) + \beta t \tag{4.24}$$

and use Green's theorem to get

$$\langle v, \phi_t \rangle + \left\langle v(w + \beta t) - A(ve^{kt})^{\gamma+1}, \phi_x \right\rangle = -\oint v_L \phi dx + \left(v_L(w_L + \beta t) - A(v_L e^{kt})^{\gamma+1} \right) \phi dt$$

$$-\oint -v_R \phi dx + \left(v_R(w_R + \beta t) - A(v_R e^{kt})^{\gamma+1} \right) \phi dt + \int_0^\infty \omega_1 d\phi = 0$$

$$(4.25)$$

and

$$\langle vw, \phi_t \rangle + \left\langle v(w + \beta t)w - A(ve^{kt})^{\gamma+1}w, \phi_x \right\rangle = -\oint v_L w_L \phi dx + \left(v_L(w_L + \beta t)w_L - A(v_L e^{kt})^{\gamma+1}w_L\right) \phi dt$$

$$-\oint -v_R w_R \phi dx + \left(v_R(w_R + \beta t)w_R - A(v_R e^{kt})^{\gamma+1}w_R\right) \phi dt + \int_0^\infty \omega_1 w_\delta d\phi = 0 \qquad (4.26)$$

If we also require

$$\begin{cases}
\frac{d\omega_{1}}{dt} = \left[v(w+\beta t) - A(ve^{kt})^{\gamma+1}\right]_{\text{jump}} - [v]_{\text{jump}}\sigma(t), \\
\frac{d}{dt}(\omega_{1}\omega_{\delta}) = \left[vw(w+\beta t) - Aw(ve^{kt})^{\gamma+1}\right]_{\text{jump}} - [vw]_{\text{jump}}\sigma(t),
\end{cases}$$
(4.27)

then (v, w) satisfies the system in the sense of distributions. Similar to the $\eta \neq k$ case, we return to the original variables ρ_L , ρ_R , u_L , and u_R , integrate the equations, subtract one from the product of the other, and let $g(t) = \int_0^t \omega_\delta(s) \, ds$ to form the ODE:

$$-(\rho_{L} - \rho_{R})g'(t)g(t) + g'(t)\left((\rho_{L}u_{L} - \rho_{R}u_{R})t - A\left(\frac{e^{k(\gamma+1)t} - 1}{k(\gamma+1)}\right)\left(\rho_{L}^{\gamma+1} - \rho_{R}^{\gamma+1}\right)\right) + (\rho_{L}u_{L} - \rho_{R}u_{R})g(t) - \left(\rho_{L}u_{L}^{2} - \rho_{R}u_{R}^{2}\right)t + A\left(\frac{e^{k(\gamma+1)t} - 1}{k(\gamma+1)}\right)\left(\rho_{L}^{\gamma+1}u_{L} - \rho_{R}^{\gamma+1}u_{R}\right) = 0.$$

$$(4.28)$$

When $\rho_L = \rho_R$, this equation can be solved explicitly:

$$\omega_{\delta} = \frac{1}{2} (u_L + u_R) - \frac{kt(\gamma + 1)\rho_L^{\gamma} A e^{k(\gamma + 1)t} - \rho_L^{\gamma} A e^{k(\gamma + 1)t} + A\rho_L^{\gamma}}{t^2 k^2 (\gamma + 1)^2}.$$
(4.29)

When $\gamma \neq -1$ and $\rho_L \neq \rho_R$, the equation is solved numerically to be similar to Fig. 18. Furthermore, the overcompressible regions are based on a simplified version of (4.17), so they match with the $\eta \neq k$ case. They also shift identically since the regions are identical to the $\eta \neq k$ case.

V. SINGULAR SOLUTION IN THE ORIGINAL VARIABLES

Now that the cases have been generally solved for, we ensure consistency with the original balance equations.

A. Case $\eta \neq k$

When we return to the original variables, the delta-shock solution is represented in the following way:

$$(\rho, u)(x, t) = \begin{cases} \left(\rho_L e^{kt}, \left(u_L + \frac{\beta}{\eta - k}\right) e^{(\eta - k)t} - \frac{\beta}{\eta - k}\right), & x < x(t), \\ (\bar{\omega}(t)\delta(x - x(t)), u_{\delta}(t)), & x = x(t), \end{cases}$$

$$\left(\rho_R e^{kt}, \left(u_R + \frac{\beta}{\eta - k}\right) e^{(\eta - k)t} - \frac{\beta}{\eta - k}\right), \quad x > x(t),$$

$$(5.1)$$

where $\bar{\omega}(t) = \omega_1(t)e^{kt}$. Converting (4.6), (4.9), and (4.10), we get

$$\frac{d\omega_{1}}{dt} = e^{-kt} \frac{d\bar{\omega}}{dt} - \bar{\omega}ke^{-kt}$$

$$= -(\rho_{L} - \rho_{R})u_{\delta}(t) + \rho_{L} \left(u_{L} + \frac{\beta}{\eta - k}\right)e^{(\eta - k)t} - \frac{\rho_{L}\beta}{\eta - k} - A(\rho_{L}e^{kt})^{\gamma + 1}e^{(\eta - k)t}$$

$$- \rho_{R} \left(u_{R} + \frac{\beta}{\eta - k}\right)e^{(\eta - k)t} + \frac{\rho_{R}\beta}{\eta - k} - A(\rho_{R}e^{kt})^{\gamma + 1}e^{(\eta - k)t}, \qquad (5.2)$$

$$\frac{d}{dt} \left(\omega_{1} \left(\omega_{\delta} + \frac{\beta}{\eta - k}\right)\right) = \frac{d}{dt} \left(\bar{\omega}e^{-kt} \left(u_{\delta} + \frac{\beta}{\eta - k}\right)e^{-(\eta - k)t}\right)$$

$$= -\left(\rho_{L} \left(u_{L} + \frac{\beta}{\eta - k}\right) - \rho_{R} \left(u_{R} + \frac{\beta}{\eta - k}\right)\right)u_{\delta}(t) + \left(\left(u_{L} + \frac{\beta}{\eta - k}\right)^{2}\rho_{L}e^{(\eta - k)t} - \left(u_{L} + \frac{\beta}{\eta - k}\right)e^{(\eta - k)t}A(v_{L}e^{kt})^{\gamma + 1}$$

$$-\frac{\beta}{\eta - k} \left(u_{L} + \frac{\beta}{\eta - k}\right)\rho_{L} + \frac{\beta}{\eta - k} \left(u_{R} + \frac{\beta}{\eta - k}\right)\rho_{R} - \left(u_{R} + \frac{\beta}{\eta - k}\right)^{2}\rho_{R}e^{(\eta - k)t} + \left(u_{R} + \frac{\beta}{\eta - k}\right)e^{(\eta - k)t}A(v_{R}e^{kt})^{\gamma + 1}\right), \qquad (5.3)$$

producing

$$\frac{dx}{dt} = u_{\delta},\tag{5.4}$$

$$\frac{d\bar{\omega}}{dt} = k\bar{\omega}(t) - \left[\rho\right]_{\text{jump}} u_{\delta}(t) + \left[\rho u\right]_{\text{jump}} - A\left[\rho^{\gamma+1}\right]_{\text{jump}} e^{nt},\tag{5.5}$$

and

$$\frac{d}{dt}(\bar{\omega}u_{\delta}) = \eta \bar{\omega}(t)u_{\delta} + \beta \bar{\omega}(t) - \left[\rho u\right]_{\text{jump}} u_{\delta} + \left[\rho u^{2}\right]_{\text{jump}} - A\left[\rho^{\gamma+1}u\right]_{\text{jump}} e^{\eta t}.$$
(5.6)

Substituting u and ρ into the delta-shock definition to verify that the solution satisfies the equations in the sense of distributions yields

$$\begin{cases}
\langle \rho, \phi_t \rangle + \langle \rho u - A \rho^{\gamma + 1} e^{\eta t}, \phi_x \rangle = -\langle k \rho, \phi \rangle, \\
\langle \rho u, \phi_t \rangle + \langle \rho u^2 - A u \rho^{\gamma + 1} e^{\eta t}, \phi_x \rangle = -\langle \eta \rho u, \phi \rangle - \langle \beta \rho, \phi \rangle.
\end{cases}$$
(5.7)

Only the proof of the second equality is presented. The first can be shown to hold by a similar argument. Let

$$\begin{cases}
Q = \langle \rho u, \phi_t \rangle + \langle \rho u^2 - A u \rho^{\gamma + 1} e^{\eta t}, \phi_x \rangle, \\
R = -\langle \eta \rho u, \phi \rangle - \langle \beta \rho, \phi \rangle,
\end{cases}$$
(5.8)

then

$$Q = \int_{0}^{\infty} \int_{-\infty}^{x(t)} \rho_{L} e^{kt} \left(\left(u_{L} + \frac{\beta}{\eta - k} \right) e^{(\eta - k)t} - \frac{\beta}{\eta - k} \right) \phi_{t} dx dt + \int_{0}^{\infty} \int_{x(t)}^{\infty} \rho_{R} e^{kt} \left(\left(u_{R} + \frac{\beta}{\eta - k} \right) e^{(\eta - k)t} - \frac{\beta}{\eta - k} \right) \phi_{t} dx dt$$

$$+ \int_{0}^{\infty} \int_{-\infty}^{x(t)} \rho_{L} e^{kt} \left(\left(u_{L} + \frac{\beta}{\eta - k} \right) e^{(\eta - k)t} - \frac{\beta}{\eta - k} \right)^{2} \phi_{x} dx dt + \int_{0}^{\infty} \int_{x(t)}^{\infty} \rho_{R} e^{kt} \left(\left(u_{R} + \frac{\beta}{\eta - k} \right) e^{(\eta - k)t} - \frac{\beta}{\eta - k} \right)^{2} \phi_{x} dx dt$$

$$- A \int_{0}^{\infty} \int_{-\infty}^{x(t)} (\rho_{L} e^{kt})^{\gamma + 1} \left(\left(u_{L} + \frac{\beta}{\eta - k} e^{(\eta - k)t} \right) - \frac{\beta}{\eta - k} \right) e^{\eta t} \phi_{x} dx dt - A \int_{0}^{\infty} \int_{-\infty}^{x(t)} (\rho_{R} e^{kt})^{\gamma + 1} \left(\left(u_{R} + \frac{\beta}{\eta - k} \right) e^{(\eta - k)t} - \frac{\beta}{\eta - k} \right) e^{\eta t} \phi_{x} dx dt$$

$$+ \int_{0}^{\infty} \bar{\omega} u_{\delta} (\phi_{t} + u_{\delta} \phi_{x}) dt.$$

$$(5.9)$$

If we assume that $\frac{dx}{dt} > 0$ for $t \in \mathbb{R}^+$ (we employ a similar argument in the case $\frac{dx}{dt} < 0$), then an inverse of x(t) exists. Thus,

$$Q = \int_{0}^{\infty} \int_{t(x)}^{\infty} \rho_{L} e^{kt} \left(\left(u_{L} + \frac{\beta}{\eta - k} \right) e^{(\eta - k)t} - \frac{\beta}{\eta - k} \right) \phi_{t} dt dx + \int_{0}^{\infty} \int_{0}^{t(x)} \rho_{R} e^{kt} \left(\left(u_{R} + \frac{\beta}{\eta - k} \right) e^{(\eta - k)t} - \frac{\beta}{\eta - k} \right) \phi_{t} dt dx$$

$$+ \int_{0}^{\infty} \int_{-\infty}^{x(t)} \rho_{L} e^{kt} \left(\left(u_{L} + \frac{\beta}{\eta - k} \right) e^{(\eta - k)t} - \frac{\beta}{\eta - k} \right)^{2} \phi_{x} dx dt + \int_{0}^{\infty} \int_{x(t)}^{\infty} \rho_{R} e^{kt} \left(\left(u_{R} + \frac{\beta}{\eta - k} \right) e^{(\eta - k)t} - \frac{\beta}{\eta - k} \right)^{2} \phi_{x} dx dt$$

$$- A \int_{0}^{\infty} \int_{-\infty}^{x(t)} (\rho_{L} e^{kt})^{\gamma + 1} \left(\left(u_{L} + \frac{\beta}{\eta - k} e^{(\eta - k)t} \right) - \frac{\beta}{\eta - k} \right) e^{\eta t} \phi_{x} dx dt$$

$$- A \int_{0}^{\infty} \int_{x(t)}^{\infty} (\rho_{R} e^{kt})^{\gamma + 1} \left(\left(u_{R} + \frac{\beta}{\eta - k} \right) e^{(\eta - k)t} - \frac{\beta}{\eta - k} \right) e^{\eta t} \phi_{x} dx dt + \int_{0}^{\infty} \bar{\omega} u_{\delta} d\phi. \tag{5.10}$$

After an integration by parts, we deduce

$$Q = -\eta \int_{0}^{\infty} \int_{t(x)}^{\infty} \rho_{L} e^{\eta t} \left(\left(u_{L} + \frac{\beta}{\eta - k} \right) e^{(\eta - k)t} - \frac{\beta}{\eta - k} \right) \phi dt dx - \beta \int_{0}^{\infty} \int_{t(x)}^{\infty} \rho_{L} e^{kt} \phi dt dx$$

$$-\beta \int_{0}^{\infty} \int_{0}^{t(x)} \rho_{R} e^{kt} \phi dt dx - \eta \int_{0}^{\infty} \int_{0}^{t(x)} \rho_{R} e^{kt} \left(\left(u_{R} + \frac{\beta}{\eta - k} \right) e^{(\eta - k)t} - \frac{\beta}{\eta - k} \right) \phi dt dx + \int_{0}^{\infty} N(t) \phi(x(t), t) dt, \tag{5.11}$$

where

$$\begin{split} N(t) &= \left(\rho_{+}e^{kt}\left(\left(u_{+} + \frac{\beta}{\eta - k}\right)e^{(\eta - k)t} - \frac{\beta}{\eta - k}\right) - \rho_{-}e^{kt}\left(\left(u_{-} + \frac{\beta}{\eta - k}\right)e^{(\eta - k)t} - \frac{\beta}{\eta - k}\right)\right)u_{\delta} \\ &+ \rho_{-}e^{kt}\left(\left(u_{-} + \frac{\beta}{\eta - k}\right)e^{(\eta - k)t} - \frac{\beta}{\eta - k}\right)^{2} - Ae^{\eta t}\left(\rho_{-}e^{kt}\right)^{\gamma + 1}\left(\left(u_{-} + \frac{\beta}{\eta - k}\right)e^{(\eta - k)t} - \frac{\beta}{\eta - k}\right) \\ &- \rho_{+}e^{kt}\left(\left(u_{+} + \frac{\beta}{\eta - k}\right)e^{(\eta - k)t} - \frac{\beta}{\eta - k}\right)^{2} + Ae^{\eta t}\left(\rho_{+}e^{kt}\right)^{\gamma + 1}\left(\left(u_{+} + \frac{\beta}{\eta - k}\right)e^{(\eta - k)t} - \frac{\beta}{\eta - k}\right) - \frac{d}{dt}(\bar{\omega}(t)u_{\delta}) \\ &= -\left[\rho u\right]_{\text{jump}}u_{\delta} + \left[\rho u^{2} - Ae^{\eta t}\rho^{\gamma + 1}u\right]_{\text{jump}} - \frac{d}{dt}(\bar{\omega}(t)u_{\delta})^{\text{by}(V.6)} - \eta\bar{\omega}u_{\delta} - \beta\bar{\omega}(t). \end{split} \tag{5.12}$$

We can easily conclude that Q = R as desired, so the equations are satisfied in the sense of distributions. Now consider the case given in Fig. 39. If x = x(t) is a curve, as shown in Fig. 39, the earlier proof needs to be modified. If there are more points at which x'(t) = 0, the proof is similar. The proof can be modified by breaking up Q as follows:

After an integration by parts and change of variables by using (5.4), we once again conclude that Q = R. For a strictly overcompressive delta-shock solution connecting a left state (ρ_L , u_L) and a right state (ρ_R , u_R), we require

$$u_R - A\rho_R^{\gamma} e^{\eta t} < u_{\delta} < u_L - A\rho_I^{\gamma} e^{\eta t} (\gamma + 1). \tag{5.14}$$

B. Case n=k

In this case, the delta-shock solution is represented in the following way

$$(\rho, u)(x, t) = \begin{cases} (\rho_L e^{kt}, u_L + \beta t), & x < x(t), \\ (\bar{\omega}(t)\delta(x - x(t)), u_{\delta}(t)), & x = x(t), \\ (\rho_R e^{kt}, u_R + \beta t), & x > x(t), \end{cases}$$
(5.15)

where $\bar{\omega}(t) = \omega_1(t)e^{kt}$. From (4.24) and (4.27), we get

$$\frac{dx}{dt} = \sigma(t) = u_{\delta} \tag{5.16}$$

and

$$\begin{cases}
\frac{d\omega_{1}}{dt} = e^{-kt} \frac{d\bar{\omega}}{dt} - \bar{\omega}ke^{-kt} = -(v_{L} - v_{R})\sigma(t) + \rho_{L}(w_{L} + \beta t) - A(\rho_{L}e^{kt})^{\gamma+1} - \rho_{R}(w_{R} + \beta t) + A(\rho_{R}e^{kt})^{\gamma+1} \\
\Rightarrow \frac{d\bar{\omega}}{dt} = k\bar{\omega}(t) - [\rho]_{\text{jump}} + [\rho u - A\rho^{\gamma+1}e^{kt}]_{\text{jump}}, \\
\frac{d}{dt}(\bar{\omega}e^{-kt}(u_{\delta} - \beta t)) = -(v_{L}w_{L} - v_{R}w_{R})u_{\delta} + v_{L}(w_{L} + \beta t)w_{L} - Av_{L}^{\gamma+1}e^{kt(\gamma+1)}w_{L} - v_{R}(w_{R} + \beta t)w_{R} + Av_{R}^{\gamma+1}e^{kt(\gamma+1)}w_{R} \\
\Rightarrow \frac{d}{dt}(\bar{\omega}u_{\delta}) = k\bar{\omega}(t)u_{\delta} - [\rho u]_{\text{jump}}u_{\delta} + [\rho u^{2} - A\rho^{\gamma+1}e^{kt}u]_{\text{jump}} + \bar{\omega}\beta,
\end{cases} (5.17)$$

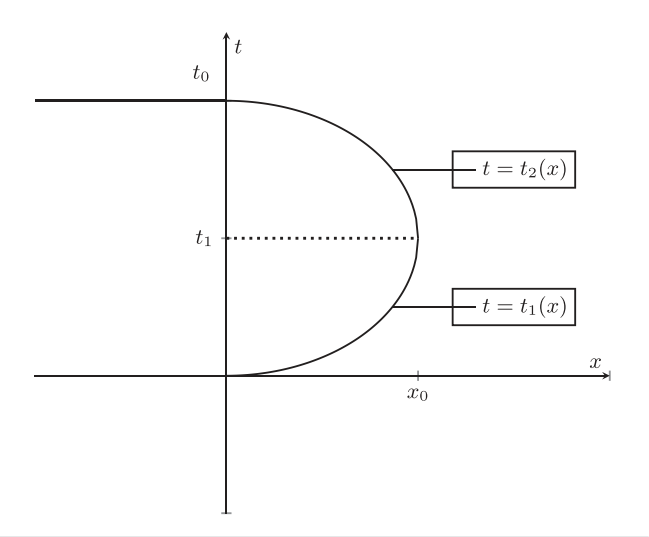


FIG. 39. Graph of an example where $x'(t_1) = 0$.

respectively. All remaining proofs for $\eta=k$ follow precisely the $\eta\neq k$ case, including those for the definitions of delta-shocks and overcompressive regions.

VI. CONCLUSION

In this work, we studied the Riemann problem of a non-symmetric Keyfitz–Kranzer type system with varying generalized Chaplygin gas. While there is a substantial body of literature on the Chaplygin gas and, more recently, on the varying Chaplygin gas (see Ref. 3), our study takes a unique approach and combines various models. We address the open question of whether classical and non-classical (delta-shocks) solutions are possible in the presence of a power γ in the density.

We provide an affirmative answer by deriving various regions in four cases [depending on the sign of $k(\gamma+1)$ and whether γ is less or greater than -1], where the Riemann problem can be solved classically (by using a one-shock, two-rarefaction, two-contact discontinuity) or non-classically (by using a combination of classical waves and a delta-shock, or solely a delta-shock). We observe that these regions shift in time. Therefore, a Riemann problem with a given left and right state can have different solutions over several time intervals. We also prove that the singular solution (which involves a delta-shock) satisfies our system in the sense of distributions. More generally, the results highlight the challenge of solving the Riemann problem for a non-autonomous system of balance laws (presence of source terms) due to the lack of self-similarity and direct dependence on the time of the wave curves, which causes region shifts.

Finally, our robust numerical evidence indicates the existence of regions where the solution consists of a two-rarefaction followed by a two-contact discontinuity (in that specific order), which we have not verified analytically, and regions where the solutions consist of a combination of a classical wave and a delta-shock. We verified the feasibility of the Local Lax–Friedrichs method for time-dependent solutions by manipulating key parameters to study changes in time. Future work will pursue these and other questions, such as uniqueness (see Refs. 32–35) and how these Riemann solutions can be used as building blocks in solving general Cauchy problems.

ACKNOWLEDGMENTS

This work is supported by the National Science Foundation under Grant Number DMS-2349040 (PI: Tsikkou). Any opinions, findings, and conclusions or recommendations expressed in this material are those of the authors and do not necessarily reflect the views of the National Science Foundation.

The authors thank Barbara Lee Keyfitz for providing MATLAB code that served as a basis for the numerical analysis done in this paper. In addition, the authors would like to express their gratitude to the reviewers for dedicating their time and effort to review the manuscript. They genuinely appreciate all of their valuable comments and suggestions, which have contributed to the enhancement of its quality.

AUTHOR DECLARATIONS Conflict of Interest

The authors have no conflicts to disclose.

Author Contributions

J. Frew: Conceptualization (supporting); Writing – original draft (supporting); Writing – review & editing (equal). N. Keyser: Conceptualization (supporting); Data curation (equal); Writing – original draft (lead); Writing – review & editing (equal). E. Kim: Conceptualization (supporting); Writing – original draft (supporting); Writing – review & editing (equal). G. Paddock: Conceptualization (supporting); Writing – original draft (supporting); Writing – review & editing (equal). C. Toumbleston: Conceptualization (supporting); Data curation (equal); Writing – original draft (supporting); Writing – review & editing (equal). S. Wilson: Conceptualization (supporting); Data curation (equal); Writing – original draft (supporting); Writing – review & editing (equal). C. Tsikkou: Conceptualization (lead); Funding acquisition (lead); Supervision (lead); Writing – original draft (supporting); Writing – review & editing (equal).

DATA AVAILABILITY

The data that support the findings of this study are available from the corresponding author upon reasonable request.

REFERENCES

- ¹M. Khurshudyan, "Can an interacting varying Chaplygin gas and tachyonic matter accelerate universe," Int. J. Geom. Methods Mod. Phys. 15, 1850155 (2018).
- ²T. C. Lipscombe, "Self-gravitating clouds of generalized Chaplygin and modified anti-Chaplygin gases," Phys. Scr. **83**, 035901 (2011).
- 3 S. Li, "Delta-shocks for a 2 \times 2 balance system of Keyfitz–Kranzer type with varying Chaplygin gas," Phys. Fluids 35, 076108 (2023).
- ⁴A. A. Sen and R. J. Scherrer, "Generalizing the generalized Chaplygin gas," Phys. Rev. D 72, 063511 (2005).
- ⁵B. L. Keyfitz and H. C. Kranzer, "Nonlinear hyperbolic problems," in A Viscosity Approximation to a System of Conservation Laws with No Classical Riemann Solution (Springer, Berlin, 1989), pp. 185–197.
- ⁶B. L. Keyfitz and H. C. Kranzer, "Spaces of weighted measures for conservation laws with singular shock solutions," J. Differential Equations 118, 420–451 (1995).
- ⁷H. C. Kranzer and B. L. Keyfitz, "Nonlinear evolution equations that change type," in *A Strictly Hyperbolic System of Conservation Laws Admitting Singular Shocks* (Springer, New York, 1990), pp. 107–125.

- ⁸M. Sever, Distribution Solutions of Nonlinear Systems of Conservation Laws (American Mathematical Society, 2007), pp. 1–163.
- 9S. Schecter, "Existence of Dafermos profiles for singular shocks," J. Differential Equations 205, 185 (2004).
- ¹⁰N. Fenichel, "Geometric singular perturbation theory for ordinary differential equations," J. Differential Equations 31, 53–98 (1979).
- ¹¹C. K. R. T. Jones, "Dynamical systems," in Geometric Singular Perturbation Theory (Springer, Berlin, 1995), pp. 44–118.
- ¹²T. H. Hsu, "Viscous singular shock profiles for a system of conservation laws modeling two-phase flow," J. Differential Equations 261, 2300–2333 (2016).
- ¹³H. Kalisch and D. Mitrovic, "Singular solutions of a fully nonlinear 2 x 2 system of conservation laws," Proc. Edinburgh Math Soc. 55, 711–729 (2012).
- ¹⁴B. L. Keyfitz, "Mathematical properties of nonhyperbolic models for incompressible two-phase flow," in *Proceedings of the Fourth International Conference on Multiphase Flow* (Elsevier, 2001).
- ¹⁵B. L. Keyfitz, R. Sanders, and M. Sever, "Lack of hyperbolicity in the two-fluid model for two-phase incompressible flow," Discrete Contin. Dyn. Syst. 3, 541–563 (2003)
- ¹⁶B. L. Keyfitz, M. Sever, and F. Zhang, "Viscous singular shock structure for a nonhyperbolic two-fluid model," Nonlinearity 17, 1731–1747 (2004).
- ¹⁷B. L. Keyfitz and C. Tsikkou, "Conserving the wrong variables in gas dynamics: A Riemann solution with singular shocks," Quart. Appl. Math. 70, 407–436 (2012).
- ¹⁸H. A. Levine and B. D. Sleeman, "A system of reaction diffusion equations arising in the theory of reinforced random walks," SIAM J. Appl. Math. 57, 683–730 (1997).
- ¹⁹ A. Mavromoustaki and A. L. Bertozzi, "Hyperbolic systems of conservation laws in gravity driven, particles-laden thin-film flows," J. Eng. Math. 88, 29–48 (2014).
- ²⁰M. Mazzotti, "Local equilibrium theory for the binary chromatography of species subject to a generalized Langmuir isotherm," Ind. Eng. Chem. Res. 45, 5332–5350 (2006).
- ²¹M. Mazzotti, "Non-classical composition fronts in nonlinear chromatography— Delta-shock," Ind. Eng. Chem. Res. 48, 7733–7752 (2009).

- ²²M. Mazzotti, A. Tarafder, J. Cornel, F. Gritti, and G. Guiochon, "Experimental evidence of a delta-shock in nonlinear chromatography," J. Chromatogr. A 1217, 2002–2012 (2002).
- ²³C. Tsikkou, "Singular shocks in a chromatography model," J. Math. Anal. Appl. 439, 766–797 (2016).
- ²⁴A. Aw and M. Rascle, "Resurrection of "second order" models of traffic flow," SIAM J. Appl. Math. 60, 916–938 (2000).
- 25Q. Zhang, "Concentration in the flux approximation limit of Riemann solutions to the extended Chaplygin gas equations with coulomb-like friction," J. Math. Phys. 60, 101508 (2017).
- ²⁶Q. Zhang, "Stability of Riemann solutions to pressureless Euler equations with coulomb-type friction by flux approximation," Electron. J. Differential Equations 2019, 1–22.
- ²⁷E. Tadmor, "Numerical viscosity and the entropy condition for conservative difference schemes," Math. Comp. 43, 369–381 (1984).
- ²⁸R. J. LeVeque, Numerical Methods for Conservation Laws (Birkhäuser Basel, 2012), pp. 95–135.
- ²⁹R. J. LeVeque, D. Mihalas, E. A. Dorfi, and E. Müller, *Computational Methods for Astrophysical Fluid Flow* (Springer, Berlin, Heidelberg, 1998), pp. 22–83.
- ³⁰G.-Q. Chen and H. Liu, "Formation of delta-shocks and vacuum states in the vanishing pressure limit of solutions to the Euler equations for isentropic fluids," SIAM J. Math. Anal. 34, 925–938 (2003).
- ³¹D. Tan, T. Zhang, T. Chang, and Y. Zheng, "Delta-shock waves as limits of vanishing viscosity for hyperbolic systems of conservation laws," J. Differential Equations 112, 1–32 (1994).
- 32T. Chen, A. Qu, and Z. Wang, "Existence and uniqueness of the global l1 solution of the Euler equations for Chaplygin gas," Acta Math. Sci. 41, 941–958 (2021).
- 33Y. Pang, C. Xu, and L. Shao, "The Riemann problem for the Chaplygin gas dynamics with a single-point heating source," Phys. Fluids 36, 036126 (2024).
- 34M. Nedeljkov, "Admissibility of a solution to generalized Chaplygin gas," Theor. Appl. Mech. (Belgr.) 46, 89-96 (2019).
- 35M. Nedeljkov and S. Ružičić, "On the uniqueness of solution to generalized Chaplygin gas," Discrete Contin. Dyn. Syst. 37, 4439–4460 (2017).